AFRL-RY-WP-TR-2021-0201

THE NEW BOUDARY LAYER THEORY

David Weyburne
Optoelectronics Technology Branch
Aerospace Components & Subsystems Division

SEPTEMBER 2021
Final Report

STINFO COPY

AIR FORCE RESEARCH LABORATORY
SENSORS DIRECTORATE
WRIGHT-PATTERSON AIR FORCE BASE, OH 45433-7320
AIR FORCE MATERIEL COMMAND
UNITED STATES AIR FORCE

NOTICE AND SIGNATURE PAGE

Using Government drawings, specifications, or other data included in this document for any purpose other than Government procurement does not in any way obligate the U.S. Government. The fact that the Government formulated or supplied the drawings, specifications, or other data does not license the holder or any other person or corporation; or convey any rights or permission to manufacture, use, or sell any patented invention that may relate to them.

This report was cleared for public release by the USAF 88th Air Base Wing (88 ABW) Public Affairs Office (PAO) and is available to the general public, including foreign nationals. Copies may be obtained from the Defense Technical Information Center (DTIC) (http://www.dtic.mil).

AFRL-RY-WP-TR-2021-0201 HAS BEEN REVIEWED AND IS APPROVED FOR PUBLICATION IN ACCORDANCE WITH ASSIGNED DISTRIBUTION STATEMENT.

//Signature//

DAVID T. TOMICH
Program Manager
Optoelectronics Technology Branch
Aerospace Components & Subsystems Division

//Signature//

FRED E. ARNOLD, Branch Chief
Optoelectronics Technology Branch
Aerospace Components & Subsystems Division

//Signature//

LESTER C. LONG, Lt Col, USAF
Deputy Chief
Aerospace Components & Subsystems Division
Sensors Directorate

This report is published in the interest of scientific and technical information exchange, and its publication does not constitute the Government's approval or disapproval of its ideas or findings.

*Disseminated copies will show "//Signature//" stamped or typed above the signature blocks.

REPORT DOCUMENTATION PAGE

Form Approved
OMB No. 0704-0188

1. REPORT DATE *(DD-MM-YY)*	2. REPORT TYPE	3. DATES COVERED *(From - To)*
September 2021	Final	1 December 2005 – 13 April 2015

4. TITLE AND SUBTITLE
THE NEW BOUNDARY LAYER THEORY

5a. CONTRACT NUMBER
In-house

5b. GRANT NUMBER

5c. PROGRAM ELEMENT NUMBER
N/A

6. AUTHOR(S)
David Weyburne

5d. PROJECT NUMBER
N/A

5e. TASK NUMBER
N/A

5f. WORK UNIT NUMBER
N/A

7. PERFORMING ORGANIZATION NAME(S) AND ADDRESS(ES)

Optoelectronics Technology Branch
Aerospace Components & Subsystems Division
Air Force Research Laboratory, Sensors Directorate
Wright-Patterson Air Force Base, OH 45433-7320
Air Force Materiel Command, United States Air Force

8. PERFORMING ORGANIZATION REPORT NUMBER

9. SPONSORING/MONITORING AGENCY NAME(S) AND ADDRESS(ES)

Air Force Research Laboratory
Sensors Directorate
Wright-Patterson Air Force Base, OH 45433-7320
Air Force Materiel Command
United States Air Force

Air Force Office of Scientific Research Public Affairs (AFOSR)
875 North Randolph Street, Suite 325, Room 3112
Arlington, VA 22203

10. SPONSORING/MONITORING AGENCY ACRONYM(S)
AFRL/RYDH

11. SPONSORING/MONITORING AGENCY REPORT NUMBER(S)
AFRL-RY-WP-TR-2021-0201

12. DISTRIBUTION/AVAILABILITY STATEMENT
DISTRIBUTION STATEMENT A. Approved for public release. Distribution is unlimited.

13. SUPPLEMENTARY NOTES
PAO case number AFRL-2021-2462, Clearance Date 2 July 2021. This is a work of the U.S. Government and is not subject to copyright protection in the United States. Report contains color.

14. ABSTRACT
The fluid boundary layer plays an important role in the chemical vapor deposition process used for advanced sensor technology. In particular, the thickness and composition uniformity of the deposited materials is intimately connected to the uniformity of the boundary layer formed above the substrate. Understanding the basic theory involving boundary layer formation and evolution over a heated plate is therefore a requirement. AFRL's research into the chemical vapor deposition process led to a number of new theoretical and experimental results in the field of boundary layer theory. A short summary of the new results is provided in the following Chapters.

15. SUBJECT TERMS
boundary layer theory, Blasius boundary layer, external boundary layer, laminar boundary layer, turbulent boundary layer

16. SECURITY CLASSIFICATION OF:			17. LIMITATION OF ABSTRACT:	18. NUMBER OF PAGES	19a. NAME OF RESPONSIBLE PERSON (Monitor)
a. REPORT	b. ABSTRACT	c. THIS PAGE			David Tomich
Unclassified	Unclassified	Unclassified	SAR	74	19b. TELEPHONE NUMBER *(Include Area Code)* N/A

Table of Contents

Section **Page**

Section **Page**

List of Figures

Figure **Page**

List of Tables

Table **Page**

1 SUMMARY

The development of chemical vapor deposition technology for advanced sensor technology, in part, involves the improvement of the thickness and composition uniformity of the deposited materials. The applied science aspects of the endeavor necessitated a deep dive into the basic theory involving fluid flow over a heated plate. The exploration led to the discovery of a number of new theoretical and experimental results in the field of Boundary Layer theory. The following Chapters provide a short summary of the work along with the appropriate references.

In the Boundary Layer Concept Chapter, the traditional boundary layer concept is reviewed and found to be flawed since it mixes internal and external boundary layer concepts. It is also found to be totally deficient in describing exterior flows like that for flows over a wing. A new "bounded" and "unbounded" boundary layer concept is offered as a remedy.

In the New Blasius Chapter, the often-used ploy of setting up a wind tunnel into a known Blasius flow condition is found to be flawed. In contrast, exterior laminar flow on a thin flat plate is found to be naturally described as Blasius flow.

In the *y*-Momentum Equation Chapter, the Falkner-Skan solution obtained from the *x*-momentum equation is used to calculate the normal to the wall *y*-pressure gradient using the *y*-momentum equation.

In the Boundary Layer Thickness and Shape Chapter, a new integral moment method for describing the thickness and shape of the boundary layer is outlined. The method can be applied to the velocity profile, thermal profile, pressure profile, and pressure gradient profiles.

In the Boundary Layer Similarity Chapter, a mathematical proof is offered as to the identity of the length and velocity scaling parameters for similarity to be present in any 2-D fluid boundary layer.

In the Turbulent Boundary Layer (TBL) Similarity Chapter, the research work on similarity scaling for the turbulent boundary layer for the last 70 years is reviewed and found to be flawed. As a remedy, the similarity scaling parameters that were identified in the Boundary Layer Similarity section are tested and found to give reasonable results for certain experimental wind tunnel results.

In the Origin of the Logarithmic Law of the Wall Chapter, a new turbulent boundary layer conceptualization is introduced that explains the origin of the Logarithmic Law of the Wall.

In the Prandtl Plus Scaling Chapter, the universality of the Log Law and Prandtl Plus Scaling's is examined and found to be flawed. Instead, a better inner region scaling parameter set is proposed to replace the Prandtl Plus set.

2 A NEW BOUNDARY LAYER CONCEPTUAL MODEL

The traditional boundary layer concept is found to incorrectly describe exterior boundary layer flow such as flow over a wing. The traditional approach fails to account for the boundary layer-wall induced excess mass and momentum resulting from the finite thickness of a flow impediment. There is no way to theoretically describe aerodynamic lift, for example, if you cannot correctly account for the excess mass and momentum diverted by the wing. A new "unbounded" boundary layer concept is offered as a remedy with the newer version discussed below having evolved slightly from its first implementation. The new conceptual model, combined with the moment-based boundary layer thickness approach, provides a theoretical path to aerodynamic lift.

2.1 The Traditional Boundary Layer Concept

Ludwig Prandtl's[1] boundary layer concept for steady 2-D laminar flow along a wall is often depicted as shown in Figure 1 (see, for example, Figure 7.6 in Hermann Schlichting's[2] seminal book on boundary layer theory). The fluids interaction with the plate induces a no-slip boundary condition (zero velocity at the wall). The flow velocity in the x-direction, $u(x,y)$, at a point x on the plate, monotonically increases from zero until it asymptotes to the velocity at the boundary layer edge which in this case is u_0. The boundary layer thickness $\delta(x)$, depicted as the dashed line, is the point where the velocity just reaches the asymptotic velocity u_0. Velocity profiles similar to those depicted in Figure 1 are routinely measured in wind tunnels around the world.

While the velocity profiles similar to that depicted in Figure 1 are often observed in wind tunnels, it is also a reasonable **approximate** depiction for exterior boundary layer air flow along a thin flat plate. **Figure 1 is only an approximate depiction for exterior flow since, although not widely appreciated, an exterior flow boundary layer on a flat plate goes through a peak near the boundary layer edge before asymptoting to u_0.**[3-5] For the thin flat plate case, the velocity peak near the boundary layer edge is small. The similarity of the thin flat plate exterior flow and the thin flat plate interior flow has resulted in the majority of the flow literature depicting both interior and exterior boundary layers using Figure 1. Unfortunately, this has also led to the fluid flow community treating interior and exterior boundary layers as equivalent (think wind tunnel experiments and flow on a wing in flight). This is reflected in the fact that it is impossible to find a discussion in the literature about the differences between interior and exterior boundary layers. For example, a Google search (on March 2020) of "boundary layer flow" yields 723,00 hits while a Google search of "interior boundary layer flow" yields zero hits and "exterior boundary layer flow" yields six hits. **The problem with this equivalence thinking is that Figure 1 does not come close in describing exterior boundary layer flows like flow along a wing in flight.** The velocity peak on a wing near the boundary layer edge can easily be 15% higher than u_0.

Figure 1 has a number of flaws beginning with the fact that conservation of mass and momentum means that the asymptotic velocity can never be u_0. Furthermore, the fact that the velocity in Figure 1 asymptotes without going through a maximum indicates that this is a wind tunnel type flow along a thin flat plate. This traditional depiction does not include the presence of the upper wall or some indication of the presence of a pressure gradient due to the walls. By not acknowledging the upper wall, the majority of the flow community interprets Figure 1 as an

exterior flow. Thus, Figure 1 is flawed in that it incorrectly mixes aspects of both interior flows (asymptotes to u_0, no maximum) and exterior flows (no upper boundary).

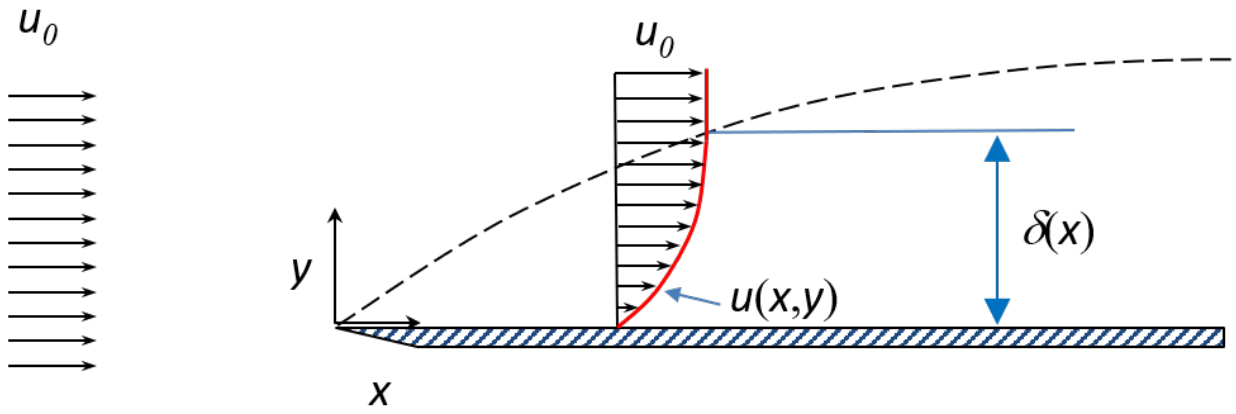

Figure 1: The Traditional Boundary Layer Model for 2-D Flow along a Thin Flat Plate

2.2 The New Bounded and Unbounded Boundary Layer Concepts

The problem with using Figure 1 for exterior flows is that this traditional boundary layer concept offers no theoretical path to describe flow phenomena like airfoil lift. It is simply not possible to correctly account for the excess mass and momentum that accumulates as the fluid flows over a finite thickness object. To correct these conceptual modeling problems, Weyburne introduced the "bounded" and "unbounded" boundary layer concepts in a series of Air Force Tech Reports[3-5] as a way to distinguish between traditional wind tunnel datasets and exterior boundary layers with a velocity peak in the near wall region.

The original bounded and unbounded concepts have subsequently evolved due to some recent simulation results. In the original model, the main difference between the bounded and unbounded concepts was that the unbounded case requires the boundary layer to go through a maximum before returning to the bulk fluid velocity u_0. However, Weyburne has done some wind tunnel simulations (discussed in more detail in Section 2.5) on a finite thickness plate and showed that even in a wind tunnel, the velocity profile can go through a maximum before returning to some constant velocity (which must be greater than u_0 to account for the mass and momentum changes induced by the presence of the boundary layers). Thus, the original bounded and unbounded division along interior versus exterior flow lines have been revised as we will see below.

Just as important as the new conceptual models is the adaption of the Integral Moment Method for describing the thickness and shape of these new boundary layer descriptions, including the peak region. It is the combination of the new model and the new thickness description that provides the theoretical path to aerodynamic lift. In what follows, the new models are reviewed and the differences are discussed.

2.2.1 The Bounded Boundary Layer Concept

The **bounded boundary layer concept** is an attempt to reframe and correct some of the deficiencies encountered in the traditional boundary layer concept used to describe wind tunnel experiments. The first step is to replace the traditional figure shown in Figure. 1 by Figure 2. The $H/2$ dashed line is added to denote this is an interior flow. All bounded boundary layers are interior flows. However, the key feature of the "bounded" boundary layer flow **is not that it is an interior flow but that it appears to asymptote to the boundary layer edge velocity $u_e(x)$ without indicating whether $u_e(x)$ is constant all the way to the top wall.** This may seem like a logically inconsistent statement since the value of $u_e(x)$ is assumed to be constant for a given x-value. This is true for a thin flat plate inserted on the centerline of a channel type wind tunnel. The $u_e(x)$ edge velocity extends from the boundary layer edge all the way to the top wall's boundary layer. However, a finite thickness plate diverts even more mass and momentum than just the boundary layer alone. This excess generates **a sizable velocity peak just above what is considered the traditional boundary layer. This peak is broad since inertia-pressure interactions are the main restorative forces. The broad peak will appear to be a plateau if measured in the traditional way.** The traditional measurement method involves measuring to maybe 2 or 3 times the boundary layer thickness values above the plate surface. However, the peak is only observable, depending on conditions, if the velocity profile is measured out to **approximately five times thicker than is traditionally measured for** velocity profiles. This point is discussed in more detail in Section 2.5. To acknowledge the fact this could be a boundary layer past a finite thickness object-plate, we have inserted a space between the velocity profile depiction and the $H/2$ dividing line. This is different than the original depiction in the earlier AF Tech Reports.[3-5]

The other major difference between Figure 1 and 2 is that the asymptotic velocity value is changed to $u_e(x)$ to acknowledge the fact that the boundary layer edge velocity can take on different values depending on the induced pressure gradients in the pipe/channel/wind tunnel. Most traditional wind tunnels all have a common feature in their implementation that allows the pressure gradient in the flow direction to be manipulated, for example, by adjusting the upper surface height, H, along the flow direction. In most wind tunnels, flows can be manipulated to have a zero-pressure gradient (ZPG), a favorable pressure gradient (FPG), or an adverse pressure gradient (APG) in the flow direction. For flow in a parallel walled channel wind tunnel, the walls induce a boundary layer pressure that becomes smaller as the flow moves along the wall. This is the FPG condition. To induce a ZPG Blasius[6]-like condition (depicted in Figure 2 with $u_e(x)$ a constant), a pressure gradient inducing mechanism, for example, slightly tilting the upper wall, needs to be adjusted to make the induced pressure gradient produced by the walls a constant along the flow direction.

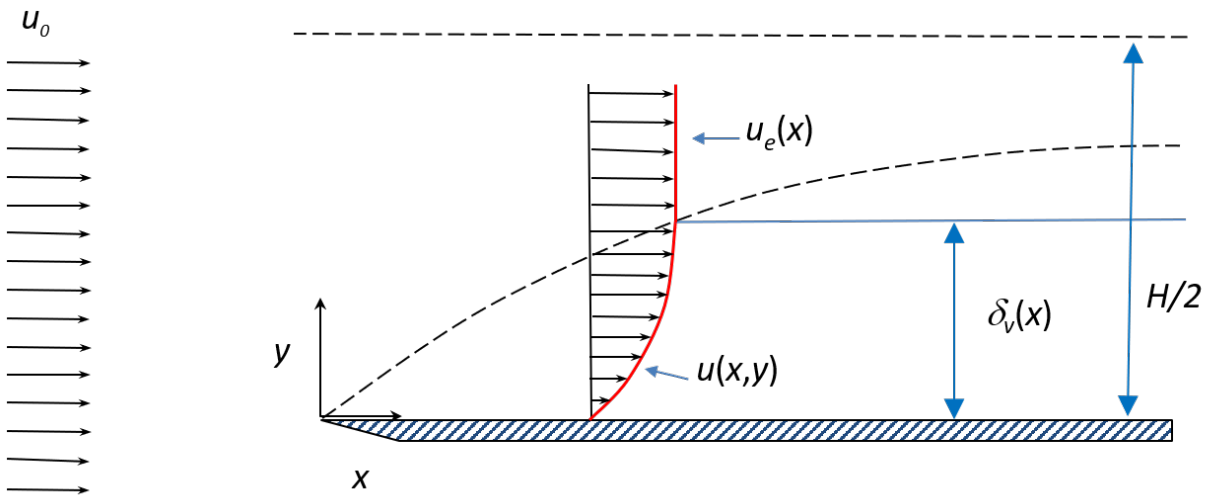

Figure 2: The Depiction of "bounded" Boundary Layer Flow in a H-gap Channel

2.2.2 The Unbounded Boundary Layer Concept

Whereas the bounded boundary layer applies to traditionally observe interior flows, the "unbounded" boundary layer, as the name implies, applies to exterior flows and some wide gap interior flows. The unbounded boundary layer concept is depicted for steady 2-D laminar flow along a flat plate in Figure 3. For the unbounded boundary layer case on a flat plate at zero-incidence angle, the important differentiating property is that velocity profile goes through a maximum near the viscous boundary layer edge and then asymptotes to the free stream velocity u_0. This is the type of boundary layer encountered for exterior flow like that for airflow over a wing in flight.

The slow rate at which the peak asymptotes to the free stream velocity means that the calculated boundary layer thickness values are much larger than the bounded boundary layer case. **A significant implication of this peaking behavior is that the 99% thickness, $\delta_{99}(x)$, becomes almost useless as a thickness parameter for the bounded boundary layer velocity profile since it no longer corresponds to any boundary layer location of consequence. It is only useful for a "thin flat plate" at zero incidence angle to the flow direction since the peak for this case will be small. For thick plates-walls, non-zero incidence angles, or most other solid surfaces, the excess flow due to the form drag of the solid object results in a near-wall peak in the velocity profile making $\delta_{99}(x)$ not useful as a boundary layer location of consequence.**

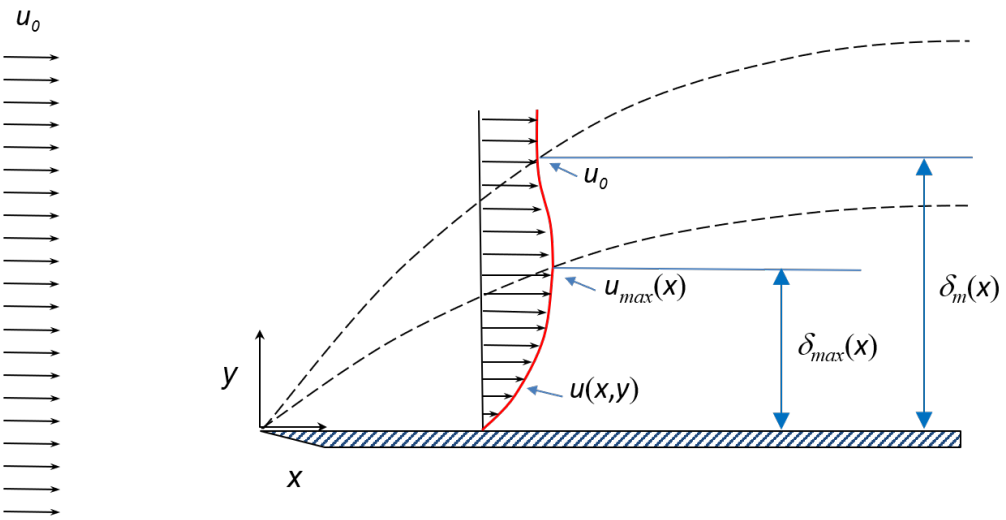

Figure 3: The Depiction of "unbounded" Boundary Layer 2-D Flow along a Plate

In the interest of providing a theoretical path to mass and momentum accountability, the unbounded boundary layer is divided into two regions: the first is the viscous region which closely mimics the traditional viscous boundary layer, and the second region which is termed the inertial region since viscous forces are mostly absent. The transition location between the two regions could be defined using the viscous thickness, $\delta_v(x)$, given by the **moment method**.[7,8] Weyburne[3] has shown that the viscous boundary layer thickness is located close to $\delta_{max}(x)$, the location of the velocity maximum u_{max}, at least for laminar flow over a wing. This boundary layer characterization method is both easy to conceptualize and is experimentally accessible. What makes this interesting is that for external laminar flow along a flat plate, this near wall region has been shown[5] to be well represented by the Blasius[6] theoretical model.

In the inertial region of the unbounded boundary layer, the velocity slowly returns to the free stream velocity from the peak value. The thickness of this inertial region is calculated using the moment method and is designated as $\delta_i(x)$.[3] Based on the limited laminar flow data that Weyburne[3] examined, the thickness of the inertial boundary layer region is hundreds to thousands of times larger than the viscous boundary layer region. This is an important differentiating property between flow past a thin flat plate and flow past an aerodynamically thick object: the "velocity" boundary layer is much thicker than the thin flat plate boundary layer due to the excess momentum which must be dissipated in the inertial region.

2.3 The Bounded and Unbounded Pressure Fields

The presence of the velocity maximum speaks to the pressure field of the boundary layer. Unfortunately, the flow community's reliance on the flawed boundary layer concept depicted in Figure 1 has resulted in a general distorted and incorrect picture of the pressure fields involved in boundary layer flow. For example, there are many examples in the literature and textbooks that incorrectly assert that the y-pressure gradient is zero in the boundary layer region.[16] The y-pressure gradient may be small, but it is definitely nonzero since the velocity normal to the wall must be nonzero. Furthermore, given the flow community's association of Figure 1 with the Blasius theoretical flow situation (see Schlichting[2] Chapter VII, for example), one might also

conclude that the x-pressure gradient in the flow direction is also zero. Hence, in the traditional interpretation of Figure 1, there are no pressure effects at all. This type of thinking has led to the generally accepted belief that the boundary layer flow situation in a wind tunnel is equivalent to external boundary layer flow. Whereas the scaled $u(x,y)$ velocity field in the flow direction can be made to look similar for the two cases, the pressure fields and the normal velocity fields are NOT equivalent.

First, consider the pressure field. In a wind tunnel, it is almost impossible to map the pressure spatially through the boundary layer region. Hence, the measured pressure fields in wind tunnels consist of simple 2-D wall pressure maps. Fortunately, flow simulation via computational fluid dynamics for laminar flow can provide the missing insights. To this end, Weyburne[3-5] did a series of 2-D laminar flow simulations in a channel. The simulations were done on a 8-meter long plate in a 2-D channel. The no-wall inlet region varied from 0.6-meter to 20-meter to fully resolve the inlet pressure field. Initially the channel gap was set at 1-meter to mimic a standard wind tunnel with a thin flat plate along the center line. In subsequent simulations the gap was increased until the flow behaved as an exterior flow using the shape of the normal $v(x,y)$ velocity profile as a test. Astonishingly, asymptotic behavior of $v(x,y)$ did not occur[3-5] until the gap was increased to 200-meters for laminar air flows with an exit Reynolds number of $Re_x=5x10^5$ (the critical laminar-turbulent transition Reynolds number)! This channel gap spacing is 2,000 times thicker than the viscous boundary layer thickness, δ_v, at mid-plate.

The pressure fields for the 1-meter and 200-meter gap 2-D channel air flow are shown in Figure 4 and Figure 5. It should be emphasized that the simulated channel flows are what is obtained for a "thin flat plate" type of boundary layer and that the peaks for even the 200-meter exterior like situation are small (~0.1%). These peaks would **not** be resolvable in a real wind tunnel. Never the less, the simulations provide valuable insights into the pressure fields. The inlet airflow in both cases is $u_0 = 0.9375$ m/s resulting in an exit Reynolds number of $5x10^5$.

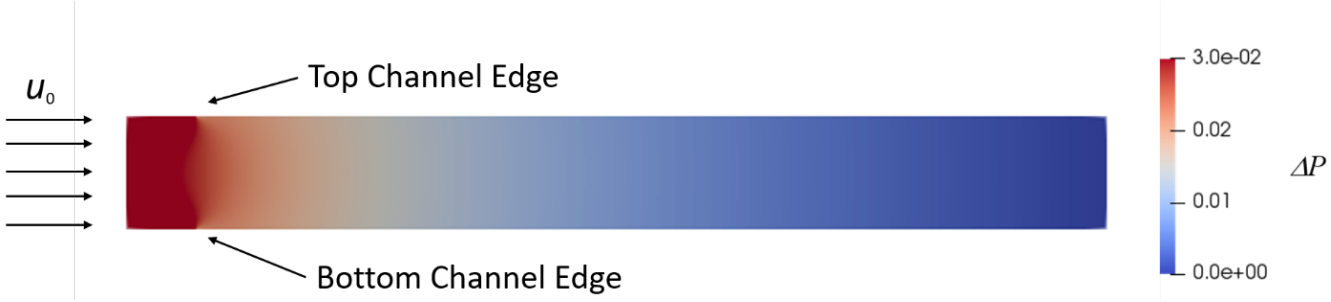

Figure 4: The Simulated Pressure Field in a 1-meter High by 8-meter Long 2-D Channel with a 0.6 Meter No-wall Inlet Region

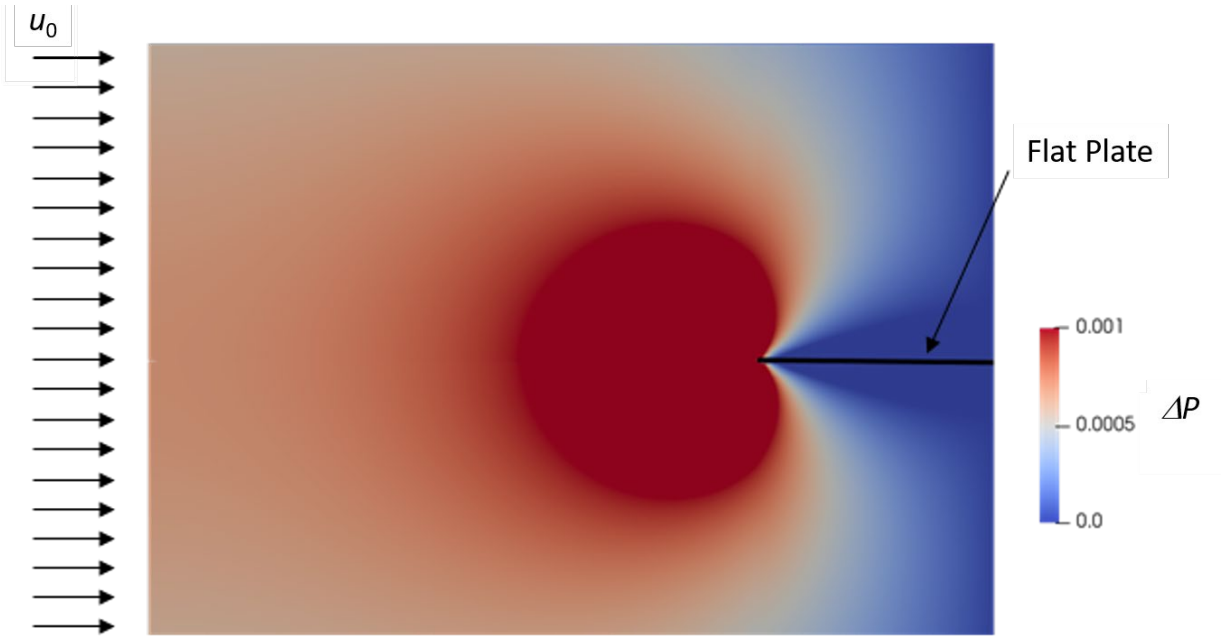

Figure 5: The Simulated Pressure Field for the Lower Channel Wall of an Exterior-like 200-meter High by 8-meter Long 2-D Channel with a 20-meter No-wall Inlet Region

The first difference to notice in the two figures is the pressure difference scales. The bounded flows pressure differences are more than an order of magnitude larger than the unbounded flow. For example, at the mid-plate (x/L=4) boundary layer edge ($y \cong 0.05$-meter), the bounded (1-meter gap) pressure is 48 times larger compared to the exterior-like unbounded (200-meter gap) mid-plate flow situation. This reflects the fact that it is much more difficult to induce flow in a thin channel then a thick channel with a fixed exit pressure requirement.

The next point to notice in the two figures is the pressure change just above the wall surface that is observable in the interior flow case whereas the exterior-like flow case shows almost no change along the channel wall. To emphasize this, the pressure difference and the x-pressure gradients near the viscous boundary layer edge (y=0.05-meter) along the plates for the two cases are shown in Figure 6. In contrast to the wind tunnel like-result (1-meter gap), the unbounded exterior-like laminar flow (200-meter gap) along a zero-incidence angle flat plate appears to be naturally in a ZPG condition (except at the front and end of the plate). More details are provided in the New Blasius Chapter.

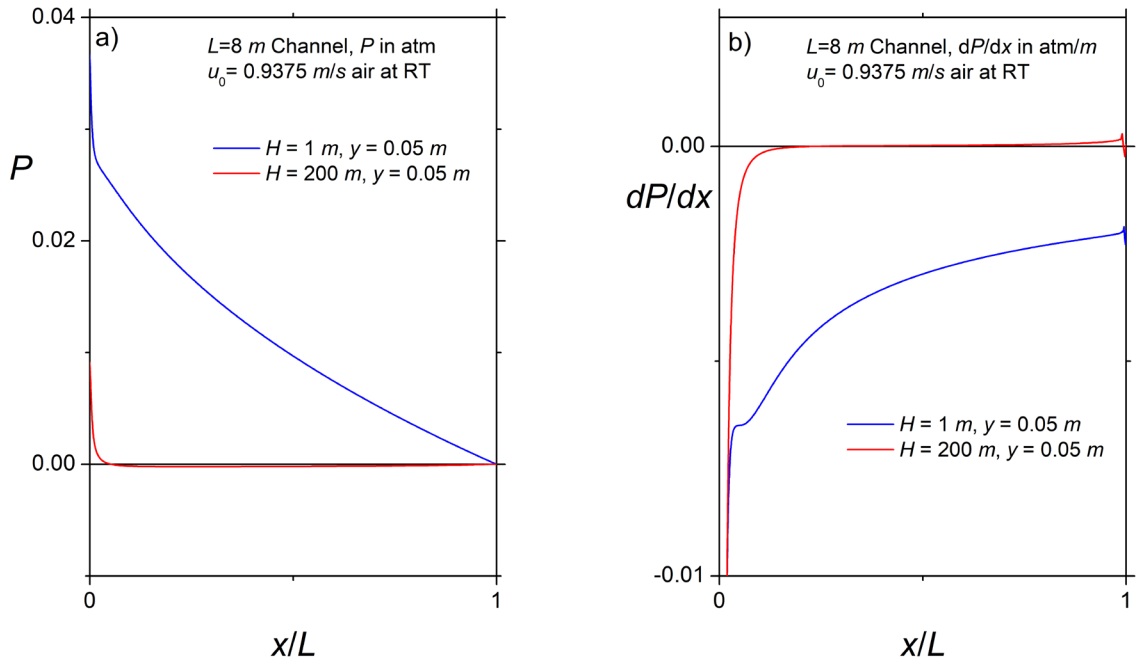

Figure 6: The Pressure at the Boundary Layer Edge for the 2-D Channels (a) and (b) *x*-pressure Gradient for the 2-D Channels

The pressure field affecting the external boundary layer (away the front edge) is very different than the interior flow case. The pressure gradient away the front edge for the external flow case appears to be primarily caused by the presence of the fast-moving free stream flow encountering the slow-moving boundary layer flow. What is usually not acknowledged is that this pressure effect must be **omnidirectional.** What this means is the pressure effect should not only manifest as the generation of a normal velocity but also generate an "excess" velocity (a velocity peak) in the flow direction. In fact, this is exactly what one sees when simulations of external laminar flows are examined. For the 200-meter external flow like case, Weyburne[5] showed that the excess maximum velocity, u_{max}-u_0, although small compared u_0, is within a factor of 2-3 of the normal velocity values in the boundary layer. The pressure gradients are the driving force for the velocities in the boundary layer. **Thus, the fact that the *y*-velocity and the excess *x*-velocity are of the same order of magnitude indicates that the *x* and *y* pressure gradients in the boundary layer region are of the same order of magnitude and that the pressure disturbance effect caused by the boundary layer is nearly omnidirectional.**

The difference between the internal and external boundary layer pressure fields also explains the behavior of the differences in the velocity at the boundary layer edge. For the 1-meter high 2-D channel, the measured **average mid-gap** and the **average boundary layer edge** *x*-pressure gradient values are essentially **the same value**. **For the 200-meter gap case, the average *x*-pressure gradient value along the plate at mid-gap is about 50 times smaller than the average *x*-pressure gradient value at the boundary layer edge.** Hence, for the bounded boundary layer, the $u(x,y)$ velocity peak is NOT observable whereas the unbounded boundary layer shows a small but detectable peak. The wall induced pressures in the wind tunnel overwhelm the boundary layer induced pressures.

In a wind tunnel, the parallel wall condition results in an FPG gradient condition as shown in Figure 6a. It is common in wind tunnels to try to generate the Blasius[6] ZPG flow condition as a "known" flow situation for certain stability or transition experiments. To do this, a pressure gradient inducing mechanism, for example, a slightly tilted upper wall, needs to be used to cancel out the naturally induced pressure gradient produced by the presence of the walls. The wind tunnel operational results using a tilted upper wall are confirmed in the 1-meter gap wedge channel simulation.[5] The simulation results indicate that a simple top wall tilt can cancel out the some of the naturally induced pressure gradient changes along the wall but not eliminate it. It merely shifts the interior pressure gradient curve in Figure 6b vertically towards a zero-pressure gradient condition. By finding the optimal tilt, the simulation scaled $u(x,y)$ velocity profiles along the plate can be made to look identical along the plate using the Blasius scaling parameters. **However**, **the normal velocity profiles and the normal pressure gradients generated under these conditions do not show similar behavior using the Blasius scaling parameters.** Hence, overall, trying to set up a Blasius flow condition in a wind tunnel based on observation of only the $u(x,y)$ velocity profile does not guarantee a "known" flow condition for stability or transition experiments as has been assumed in the past.

2.4 The Bounded and Unbounded Velocity Fields

The pressure fields are not the only differences encountered in bounded and unbounded boundary layer flows. In Figure 7, the $u(x,y)$ velocity profile for laminar flow in a 8-meter 2-D channel is plotted as a function of channel gap. It is not widely appreciated that the large gap 2-D channel flow behaves as shown in Figure 2 rather than the more widely known parabolic flow introduced in many textbooks. Parabolic flow in a channel only occurs when the gap is on the order of the viscous thickness $\delta_v(x)$ or smaller. The boundary layer thickness at mid-plate at an air velocity of 0.9375 m/s is about $\delta_v \sim 0.04$-meters for an external boundary layer ($H = 200$-meter case). The transition from parabolic flow to large gap 2-D channel flow is apparent. The profiles with channel gaps larger than 10-meters all look similar.[5]

For the flat plate unbounded air flow case (H=200 meter), the peak velocity u_{max} is only 0.1% higher than u_0. However, for a tilted plate or a wing in flight, the effect can be much larger. For example, a 0.5 Mach airflow over a NACA 0012 wing section is shown in Figure 8. This figure was extracted from a simulation by Swanson and Langer[9] in which a 4096 by 2048 mesh full

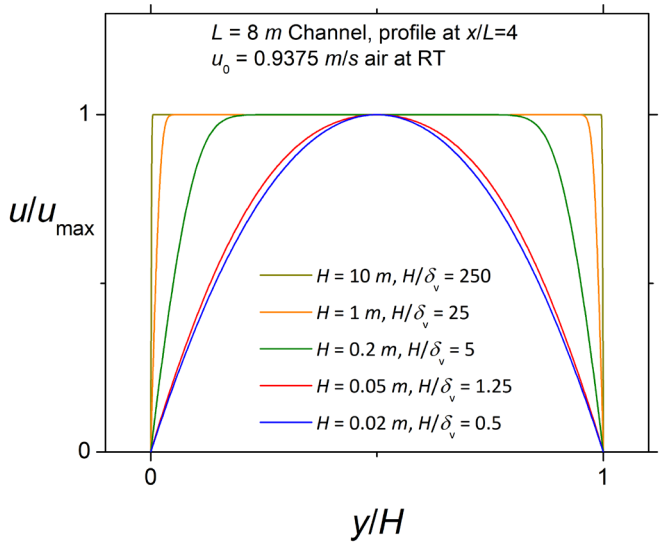

Figure 7: The *u*(*x*,*y*) Velocity Profiles in a 2-D Channel as a function of Channel Gap

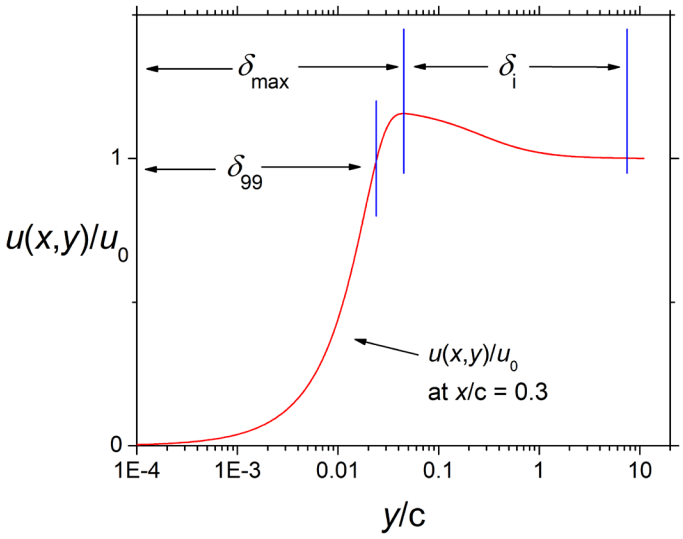

Figure 8: The Scaled u(x,y) Velocity Profile on a NACA0012 Airfoil at x/c = 0.3 According to Swanson and Langer9

Navier-Stokes compressible simulation was done around a NACA 0012 airfoil. Included in this figure are the δ_{99}, δ_i, and the δ_{max} locations. The δ_i/δ_{99} ratio value is 311, and the u_{max} value is 9% higher than the u_0 value. **The large difference between the δ_{99} and the (3-sigma) δ_i value demonstrates the inadequacy of the traditional boundary layer thickness description. Furthermore, the large velocity peak demonstrates the inadequacy of Fig. 2.1 as a boundary layer depiction for exterior flows.**

The 2-D laminar flow simulations revealed that the differences between the Blasius[6] scaled $u(x,y)$ velocity profiles along the wall in a 1-meter ZPG-like flow (**tilted wall**) and a 200-meter air gap channel are small. As one moves along the wall, the $u(x,y)$ velocity profiles plotted using

Blasius scaling show similarity behavior (see New Blasius Chapter) in both cases. **It is in the $v(x,y)$ velocity profiles and the y-pressure gradient profiles where one observes the noticeable changes.** To highlight this, in Figure 9, the normal velocity $v(x,y)$ is plotted as a function of channel gap. Using the y-scale shown, it is hard to see that all of the profiles start a value of $v(x,y=0) = 0$, and then peak at about y=0.05-meter ($\sim\delta_{max}$). The pictured y-scale is chosen to emphasize the tail regions return to zero behavior at midgap. Note that it is not until the H=200-meter case that the $v(x,y)$ velocity smoothly asymptotes to zero, just as one would expect for an external flow. The y-pressure gradient shows the same type of behavior, only showing asymptotic behavior to zero for the 200-meter case. Figure 9 emphasizes the differences in the shape of the profiles as a function of channel gap. There are also differences as one moves along the plate. This point is discussed in more detail in the New Blasius Chapter, but in summary, the 200-meter unbounded $v(x,y)$ velocity profiles show Blasius type similarity whereas the 1-meter gap bounded $v(x,y)$ velocity profiles do not as one moves along the wall.

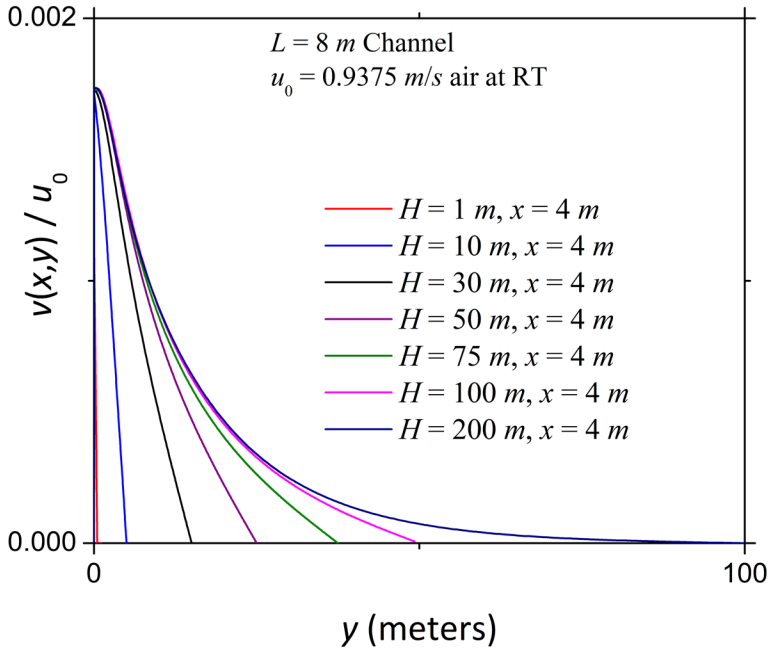

Figure 9: The Normal Velocity $v(x,y)$ in a 2-D Channel as a Function of Channel Gap

2.5 The Bounded And Unbounded Designations

The ultimate aim of this whole endeavor is to develop at boundary layer conceptual model joined together with a boundary layer thickness and shape method that allows for the complete mass and momentum accounting due to boundary layer flow. The traditional boundary layer description, and even the new "bounded" boundary layer description, does not accomplish this goal. It is not possible to account for the complete mass and momentum changes due to the presence of the wall with these descriptions. The new bounded boundary layer description is included because it gives us a way to at least describe wind tunnel experiments where complete accountability would be very difficult. On the other hand, the new **unbounded boundary layer**

description merged with the moment thickness method[7,8] for describing thickness and shape does offer a path for the complete accounting of mass and momentum, at least for exterior flows.

The bounded boundary layer description is intended to describe traditional wind tunnel boundary layers as traditionally measured. The unbounded boundary layer is intended to describe exterior boundary layers. In the original designation, Weyburne[3] used the presence of a peak as a way of differentiating bounded and unbounded. **However, one must be careful when applying that designation to describe traditional wind tunnel boundary layers as traditionally measured.** In a typical wind tunnel experiment, the data points are taken in the asymptotic region of the boundary layer to maybe 2 or 3 times the viscous boundary layer thickness value. This measured velocity plateau is just referred to $u_e(x)$. The problem is that a $u_e(x)$ plateau could be part of a velocity peak, a peak so broad that it is completely missed.

To illustrate this point, a 2-D simulation was performed on a finite thickness plate in a 2-D channel (Weyburne, unpublished results). The new simulation is based on the OpenFoam's T3A turbulence transition tutorial-verification simulation. To ensure the boundary layer was properly rendered, the number of mesh points was increased by a factor of 16 and the top boundary was turned into a wall boundary to mimic a wind tunnel. The simulation is able to reproduce Rolls-Royce[10] T3A wind tunnel wall shear stress results (not shown). It also is able to reproduce the velocity profiles.

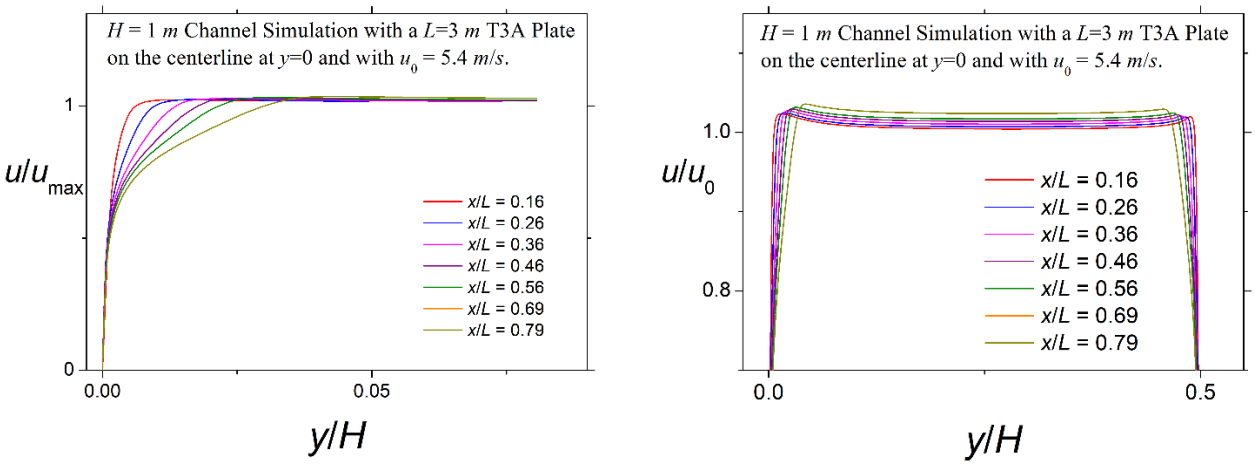

Figure 10: The Simulated Velocity Profiles for the T3A[10] Case at Different Plate Locations (a) and (b) Complete Simulation Velocity Profiles showing Velocity Peaks for the T3A[10] Case

The simulated velocity profiles are shown in Fig. 2.10. The velocity profiles in Figure 10a are intentional cut off to match the actual maximum T3A experimental[10] y-values. For comparison, in Figure 10b we show the complete velocity profile. The velocity profile scaling was switched to u_0 in order to show the full effects of the plate and walls on the profiles. The finite thickness T3A rounded nose plate resulted in a velocity peak about 2% higher than u_0. In contrast, **neither** the Rolls-Royce experimental data (not shown) **nor** the simulation result terminated at the same y-extent (Figure 10a) **show peaking behavior**. The 3-sigma[3] boundary layer thickness, δ_i, for the peaks is ~0.2H. This is about 10 times thicker than δ_{99}, for example. The largest Rolls-Royce experimental data point location is about 3 times δ_{99}. The take away from this result is

that even wind tunnel experiments involving aerodynamically thick objects will show peaking behavior of the velocity profile in a wind tunnel if the velocity profile was measured all the way from the plate to the upper wall.

A second point that complicates the designations is that there is not a sharp dividing point between interior and exterior boundary layers. The channel simulations indicate that everything from an interior to and exterior-like boundary layer condition can be generated by simply changing the channel gap. **The choice of when a flow situation should be designated interior or exterior** comes down to a choice of an appropriate criterion. One possibility is to pick an outer region velocity gradient $\mathbf{d}v(x,y)/\mathbf{d}y$ (normal velocity gradient) lower limit value (see Figure 9) to indicate when asymptotic unbounded boundary layer behavior has been achieved.

Given the complicated nature of the different boundary layer scenarios, the designations bounded and unbounded will take on the following designations: 1) the **bounded boundary layer and its associated depiction (Figure 2)** will be used to refer to interior flow wind-tunnel type boundary layers taken at the typical wind tunnel experimental extent. The boundary layer thickness for a bounded boundary layer needs clarification. If the boundary layer thickness is defined as the point above the wall where the flow no longer feels the effect of the opposing walls, then almost all interior bounded boundary layer thicknesses would be the channel width H. However, the flow community has adopted the viscous boundary layer thickness, or the turbulent broadened viscous boundary layer thickness, as the definition instead which we will also adopt to prevent confusion. 2) The **unbounded boundary layer and its associated depiction (Figure 3)** will be used to describe boundary layers on exterior walls. These boundary layer descriptions are not intended to encompass all possible boundary layer situations, just the most important and widely encountered versions.

2.6 Turbulent Boundary Layer Concept

The turbulent boundary layer adds another level of complexity to the boundary layer concept. The conceptualization of the turbulent boundary layer is addressed in another chapter (the TBL Concept Chapter) but not in the same context as used above. Turbulent flow does not have a closed form solution approach so the CFD approach used above to calculate the velocity and pressure plot fields cannot be easily applied to this case. One approximate approach is to use an approximate eddy viscosity model that can be verified against experimental results. This is the approach used in Figure 10. More work needs to be done to understand how turbulence effects mass and momentum accountability on exterior flows.

2.7 Application of the New Boundary Layer Concept to Aerodynamic Lift

In spite of over a hundred years of effort, there has never been an accepted theory of aerodynamic lift. The reason may be due to the fact that, until now, there has been way to accurately describe the boundary layer situation for flow along a wing. **Early practitioners incorrectly adopted the wind tunnel boundary layer concept** as how they believed flow over a wing behaved. This equivalence of wind tunnel and external boundary layer flow is deeply embedded in the fluid flow literature. However, for the last 50-60 years, computer flow simulations have been available which, when actually examined at even a coarse level, easily demonstrate that the traditional boundary layer concept depicted in Figure 1 does not work for

this case. The wind tunnel model with a non-peaking velocity profile simply cannot describe the added mass and momentum that occurs when the flow encounters a finite thickness obstruction in an external flow environment. The new conceptual model combined with the new moment-based boundary layer thickness and shape method[7,8] (see Chapter 5) allows one to describe the peaking behavior as well as the slow inertial return of the peak to the free stream velocity.

To demonstrate the usefulness of this process for aerodynamic applications, we revisit the 0.5 *M*, α=0, NACA0012 simulation[9] by Swanson and Langer. One of the goals of the simulation was to show that low Reynolds number (Re_c = 5000) **laminar airflow** over an airfoil could have a numerically stable solution. Examination of the boundary layer peak behavior reveals that the average peak height, $\boldsymbol{u_{max}(x)}$, over the majority of the wing surface is 13% above the free stream velocity (see Figure 2.8 for example). Weyburne[3] showed that this mostly laminar flow simulation demonstrated an important trait: the **velocity peak location**, **denoted as $\boldsymbol{\delta_{max}(x)}$,** is located close to the viscous boundary layer thickness edge, denoted as $\boldsymbol{\delta_v(x)}$. Figure 11 shows

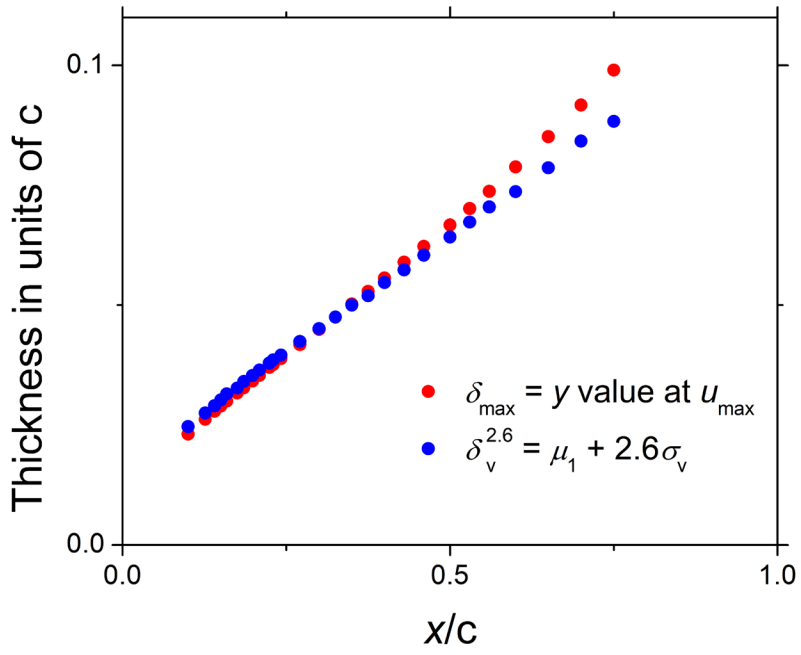

Figure 11: The *u*(*x*,*y*) Velocity Peak Location and the Viscous Thickness for 0.5 *M* Airflow Impinging a NACA0012 Wing Surface Simulation from Swanson and Langer[9]
The Leading Edge is at x/c = 0 and the Trailing Edge is at x/c = 1.

the location of the peak compared to moment based viscous thickness.[3] The δ_v value is calculated using the second derivative moment method.[7,8] Note that this particular simulation[9] has a trailing edge recirculation just above the wing surface starting at about *x*/*c*=0.8 which may explain the behavior in Figure 11 for large *x*/*c* values. The first important point to note is that this figure shows a strong correlation between this jet-like peak location and the edge of the viscous near wall thickness. Normally the moment-based thickness is described as the mean location plus 2-sigma (~99%), the 3-sigma, *etc*. depending on the application. The results in Figure 11 indicate that the velocity peak occurs just above where the viscous forces vanish. The second important takeaway from this figure is that the highest speed flow over the wing follows

the wing contour, plus the viscous thickness, along the entire wing surface. This Coandă-like effect brings into question the wide spread dismissal of this effect as an explanation for aerodynamic lift. The key to this new revelation is the combination of the new conceptual model with the moment-based thickness and shape approach which, for the first time, allows the viscous forces to be tracked. This combination allows for a much more qualitative as well as quantitative description for flow along a wing.

Aerodynamic lift is often identified as the component of force that is perpendicular to the flow direction. Obviously, an important aspect of the force is due to the pressure differences above and below the airfoil. In Figure 12, we plot a series of pressure profiles perpendicular to the flow direction along the NACA0012 wing taken from Swanson and Langer. The minimum pressure is on the order of 5% lower than atmospheric pressure at these conditions and occurs at the wings surface. The low-pressure bubble extends about five cord lengths above the wing. Not surprisingly, this is the same extent as the *u*(*x*,*y*) velocity bubble. The important take away from this figure is that the minimum pressure occurs very close to the velocity peak. The pumping action of high-speed fluid flow along a wall is similar in nature to the fluid pumping action of a flat rotating disk. What is somewhat surprising in this figure is that even near the leading edge, the pressure above the wing is negative. It is only in front of the leading edge (not shown) that the pressure is larger than atmospheric.

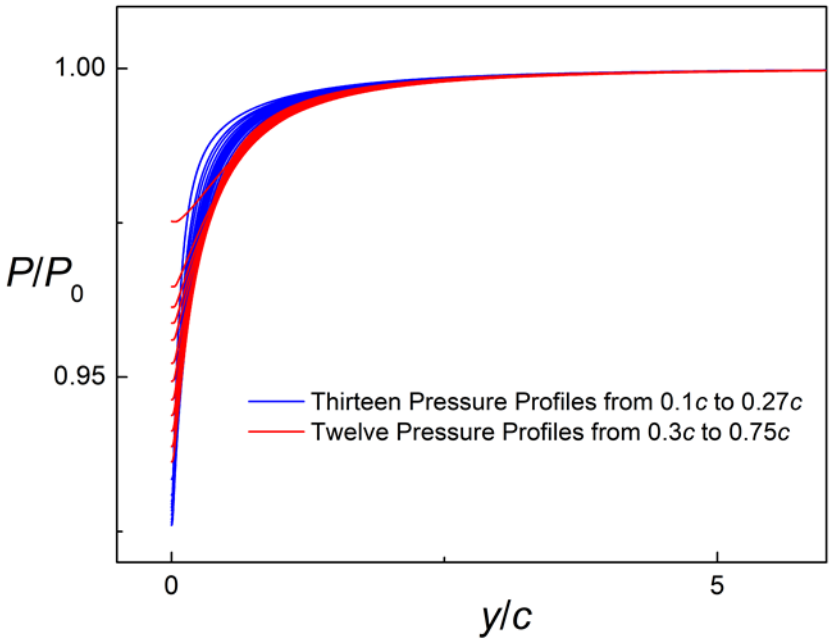

Figure 12: The Pressure Profiles along a NACA0012 Wing in a Direction Perpendicular to the Airflow

Data from a simulation by Swanson and Langer.

The insights provided by Figures 11 and 12 provide a possible path to a purely theoretical approach to aerodynamic lift. It may be possible to combine these insights with the semi-empirical panel approach of Drela and Giles[11] (XFOIL). However, more work needs to be done, particularly on the role of turbulence. Attempts to extend the δ_{max} - δ_v correlation to wings with turbulent flow is challenging since turbulent flow does not have a closed form solution. One

approximate approach is to use an approximate eddy viscosity model that can be verified against experimental results. To that end, Weyburne (unpublished preliminary results with the 1793x513 NASA mesh) used the OpenFoam Turbulent flow over NACA0012 airfoil (2D) tutorial-verification simulation to investigate the correlation between δ_{max} and δ_v. To the extent that the Spalart-Allmaras turbulence model represents the viscous region accurately, it is apparent (results not shown) that δ_{max} is much larger than δ_v, on the order of 1000 times bigger.

To try to understand the difference between the laminar and turbulent behavior, Weyburne (unpublished) modified the OpenFoam's T3A turbulence transition tutorial-verification simulation used to generate Figure 10. The Rolls-Royce[10] T3A wind tunnel simulation height was increased by a factor of 16 to 16-meters **to simulate an exterior flow** and the number of mesh points was increased by a factor of 16 times. The simulation was run with the Langtry-Menter k-omega Shear Stress Transport model and then with the turbulence model turned off. The results are shown in Figure 13. The results in Figure 13a indicate the simulation is able to reproduce the wall shear experimental results. This means the RAS model is able to correctly model the near wall region. Examining the Figure 13b results, one notices that the laminar T3A simulation results show a good correlation between δ_{max} and δ_v whereas the turbulent simulation results do not. These results support the Swanson and Langer[9] laminar results that indicate the jet-like excess flow is closely following the viscous boundary layer edge, at least for laminar flow. The turbulent velocity maximum is maybe 2-3 thicker than the laminar case but still relatively close to the plate surface. Future work needs to be done to understand these results compared to the OpenFoam's turbulent NACA0012 result.

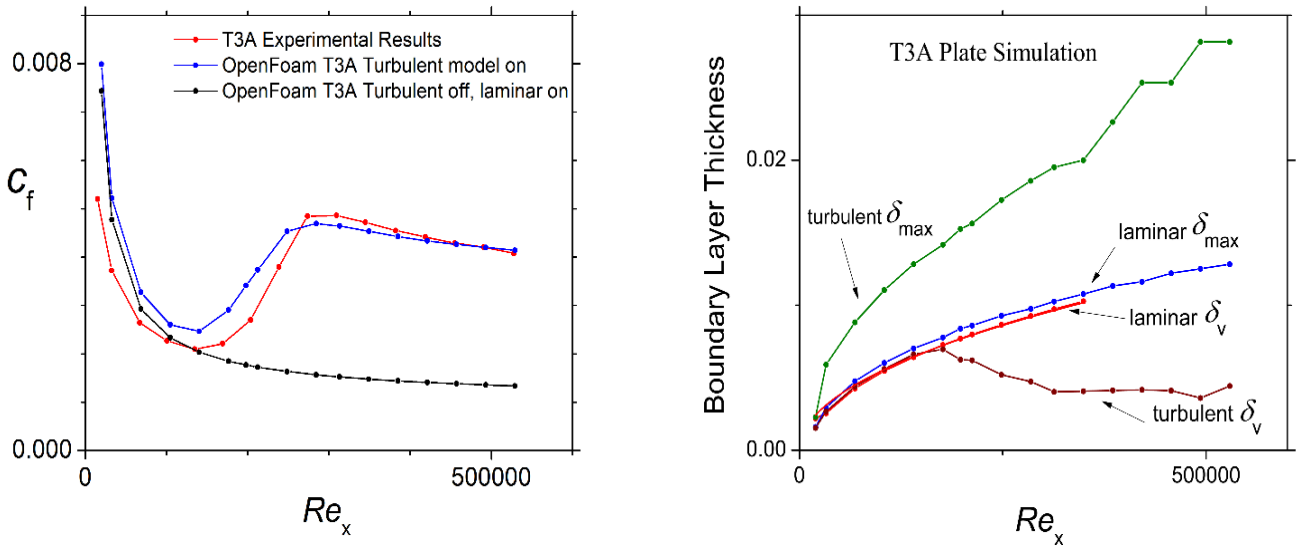

Figure 13: The Skin Friction for the T3A Experimental and Simulation Results (a) and (b) the Boundary Layer Thickness for the T3A Simulation in Units of *c*

2.8 Application to Transitional Boundary Layers

Although our goal is to develop a conceptual model combined with a boundary thickness method for describing airfoil lift, the combination has already led to an important insight into transitional boundary layers. Very little is known about the physics of transitional boundary layer flow. To

the extent that the *k*-omega Shear Stress Transport turbulence model represents the viscous region accurately, the results shown in Figure 13 provide a valuable insight into transitional boundary layers. The skin friction results in Figure 13a indicate the velocity profiles start as laminar then transition to turbulent boundary layers further along the wall. For laminar flow along a flat plate, the boundary layer thickness increases as the square root of the distance. This behavior for the "laminar δ_v" in Figure 13b is well fitted (not shown) to a simple square root function. Now consider the "turbulent δ_v" results depicted in Figure 13b. The purely laminar portion consists of the first 1 or 2 simulation points. The next 4 or 5 simulation points constitute the transitional points and the remaining data points the turbulent boundary layer simulation results. **Notice that, for the transitional boundary layer results, the viscous boundary layer thickness is still increasing as the square root of the distance along the plate (Figure 13b).** Where the transitional curve breaks is the point where this square root behavior can no longer be supported. The turbulent motion penetrates into this near wall region and relaxes the energy strain of the fluid trying to maintain this square root behavior. It is this viscous thickness behavior that characterizes transitional boundary layer behavior. The following fully turbulent boundary layers simulation points have viscous boundary layer regions that basically remain constant with Reynolds number. This is one of the defining characteristics of fully turbulent boundary layer behavior. Hence, the new conceptual model combined with the moment-method for boundary layer thickness has provided an important insight into transition boundary layer theory.

3 THE NEW BLASIUS MODEL

Wind tunnel operation often involves initial setup in the Blasius[6] flow regime as a means of operational verification. Furthermore, certain stability and transition experiments purposely use the Blasius flow as a "known" flow condition. However, this assumption of a known flow condition is flawed; the normal velocity and the normal pressure gradient often do not correspond to the Blasius flow condition. In contrast, exterior laminar flow along a flat plate is shown to be naturally described as Blasius flow.

3.1 The Blasius Model Failure

Ludwig Prandtl's[1] boundary layer concept for steady 2-D laminar flow along a wall is often depicted as starting with a zero velocity at the wall (no-slip boundary condition) which then monotonically increases above the plate until it asymptotes to the velocity at the boundary layer edge (Figure 1). Paul Richard Heinrich Blasius,[6] one of Prandtl's students, developed the theoretical model corresponding to the flow for the case where the boundary layer edge velocity is just the free stream velocity u_0. This close association with the traditional conceptual model for boundary layer flow has ensured a prominent place for the Blasius theoretical model. The Blasius model appears in almost every fluid flow textbook as an introduction to boundary layer flow as well as an introduction to similarity theoretical solutions to boundary layer flows. The universal acceptance of this model appears to be partly driven by the association between the conceptual depiction and the theoretical model, partly by the simplicity of the model, and partly by the fact that wind tunnel measurements seem to confirm its existence. The universal acceptance of the model, fueled by the wind tunnel experiments, has resulted in the Blasius theoretical model being routinely used as a way to verify proper wind tunnel configuration/operation (*e.g.* Jovanović, et al.[12]) as well as a way to verify computer flow simulation computational engines (*e.g.* Ghia, *et.* al.[13]).

The near universal acceptance of the theory is based, in part, on wind tunnel experiments beginning with Nikuradse's[14] experimental wind tunnel results featured in Schlichting's[2] seminal book on boundary layer theory (see Schlichting's Figure 9). This result would appear to be a powerful confirmation of the Blasius theory in particular and the boundary layer concept in general. However, this apparent experimental confirmation needs to be re-evaluated. Recently Weyburne[3-5] set up a series of computer simulation experiments that, in part, tried to verify the existence of Blasius type flow in a 2-D channel with typical wind tunnel dimensions (1-meter high by 8-meter long). It was found that parallel channel wall flow did not produce Blasius type flow for 2-D channel airflow at room temperature. This result appears to correspond to actual wind tunnel experiments and is not unexpected since the pressure gradient in the flow direction will not be zero under these conditions. Nikuradse[14] results, according to Schlichting,[2] employed some type of pressure gradient cancellation technique. One standard wind tunnel technique to induce a zero-pressure gradient along the tunnel plate and thereby generate Blasius profiles is to slightly tilt one of the tunnel plates to counter the built-in pressure gradient formed by the wind tunnel walls (see, for example, Jovanović, *et. al.*[12]). And, in fact, the computer simulation of a wedge shaped channel did show that it is possible to produce $u(x,y)$ velocity profiles that behaved similarly when scaled with the Blasius scaling parameters.[4,5] **However**, the same simulations indicated that the normal velocity profiles and the normal pressure gradient profiles do not show similarity using the Blasius scaling parameters. Overall, it was concluded that the

small angle wedge flow used to induce a zero-pressure gradient (ZPG) value at the boundary layer edge is not well represented by the Blasius theoretical model. Note that in typical wind tunnel experiments, neither the normal velocity profiles nor the normal pressure gradient profiles are usually measured. Hence, this experimental discrepancy has never been noticed. In any case**,** the simulation results indicate that the assumption that the Blasius theoretical model describes steady 2-D laminar flow along a tilted flat plate in a wind tunnel is not correct.

It is not only experimental verification problems that cast doubt on the Blasius theoretical model. A closer look at the Blasius model reveals a number of disturbing theoretical discrepancies that one would not expect for fluid flow along a flat plate. The most serious problem with the Blasius solution is that the calculated normal to the wall velocity and the normal to the wall pressure gradient (see *y*-momentum Chapter) are both finite at an infinite distance from the wall. This is obviously non-physical. At some point above the wall, the normal velocity and the normal *y*-pressure gradient must go to zero. The problem has been commonly ignored although there have been a number of not very satisfying attempts to explain this away (see, for example, Lewins[15]). More recently, Weyburne[5] pointed out another problem with the Blasius model. In the Blasius model, the pressure gradient in the flow direction is assumed to be zero in the boundary layer region. This assumption cannot be correct. There can be no flow without a driving force but just as problematic is that the pressure forces in the boundary layer region that induce the normal velocity flow must also affect the pressure gradient in the flow direction since pressure affects cannot be unidirectional. The consequences of this additional non-zero pressure gradient in the flow direction in the boundary layer is that there should be a velocity overshoot, a peak, near the boundary layer edge, at least for external flows. This behavior is not observed for the Blasius model as it is normally applied to boundary layer flows.

3.2 The New Blasius Theoretical Model

Our recent computer simulation experiments indicate that the Blasius[6] theoretical model no longer enjoys the wind tunnel experimental verification support that it has had in the past. Coupled with the theoretical problems just mentioned, it would appear the Blasius model has serious theoretical and experimental problems.

However, there is a way forward. Recently, Weyburne[5] reapplied the Blasius theoretical model in a context that removes all of the just mentioned problems. The key is not the theoretical model but the conceptual model for the boundary layer. In an earlier set of AF Tech Reports,[3,4] the "unbounded" and "bounded" boundary layer concepts were introduced that correspond to boundary layers formed in exterior and interior flow situations. For the unbounded boundary layer case for flow on a thin flat plate at zero incidence angle, the velocity profile goes through a small maximum near the viscous boundary layer edge and then slowly declines to the free stream velocity. This is the type of boundary layer encountered for exterior flow like that for airflow over a wing in flight. Although it is nearly impossible to measure boundary layer velocity profiles under flight conditions, it is possible to do computer simulations of exterior flow along a wall. Weyburne[5] simulated airflow along an 8-meter long channel with the gap initially set at 1-meter to mimic a standard wind tunnel and then increased until the flow behaved as an exterior flow. Astonishingly, exterior-like flow did not occur until the gap was increased to over 100-meters for laminar flows with a Reynolds number $Re_x=5x10^5$ (the critical laminar-turbulent

transition Reynolds number)! The simulations indicated that this large gap, zero-incident angle unbounded boundary layer case is naturally in a ZPG flow condition (see Figure 6b). This makes the Blasius theoretical model a good candidate for the unbounded boundary layer along a thin flat plate.

The association between the unbounded boundary layer and the Blasius theoretical model also has distinct theoretical advantages. For theoretical convenience, the unbounded boundary layer can be divided into two regions; the first is the viscous region which closely mimics the traditional viscous boundary layer, and the second region which is termed the inertial region since viscous forces are mostly absent. In a previous report,[3] it was found that there was good correspondence between the viscous boundary layer thickness, δ_v, and the location of the velocity maximum δ_{max}. **Thus, in the new conceptual model, the viscous region is taken to be located between the wall and $\boldsymbol{\delta_{max}}$ or $\boldsymbol{\delta_v}$.** This is the key to applying the Blasius theoretical model. Now there is a physical and logical justification for applying the viscous Blasius model to the just the near wall region. This division into two regions eliminates the normal to the wall velocity and the normal to the wall pressure gradient infinite extent problem. The new division also solves the velocity boundary layer edge peak problem. The net result is that the new Blasius theoretical model has a solid theoretical basis.

However, it is the experimental results that really clinch it for the new Blasius model. In Figures 14-16, examples of the velocity profiles and y-pressure gradient profiles for the bounded and unbounded and boundary layers at seven locations along the bottom plate are shown. These figures shows the $u(x,y)$ and $v(x,y)$ velocity profiles and the y-pressure gradient profile for the 1-meter gap tilted channel-wedge flow and for the 200-meter gap channel flow at various locations along the plate. The 1-meter normal velocity and normal pressure gradients displayed in Figures 15a and 16a do not show similar behavior. On the other hand, the 200-meter velocities and normal pressure gradients show good collapse to the Blasius theoretical result except for the 6 and 7 meter y-pressure gradient result. These latter results are probably due to the flow exit affects (the exit was set to zero pressure). Combining these results with the dP/dx result from Figure 6b, it is clear that the experimental results for the unbounded boundary layer (200-meter) show good correspondence to the Blasius theoretical model.

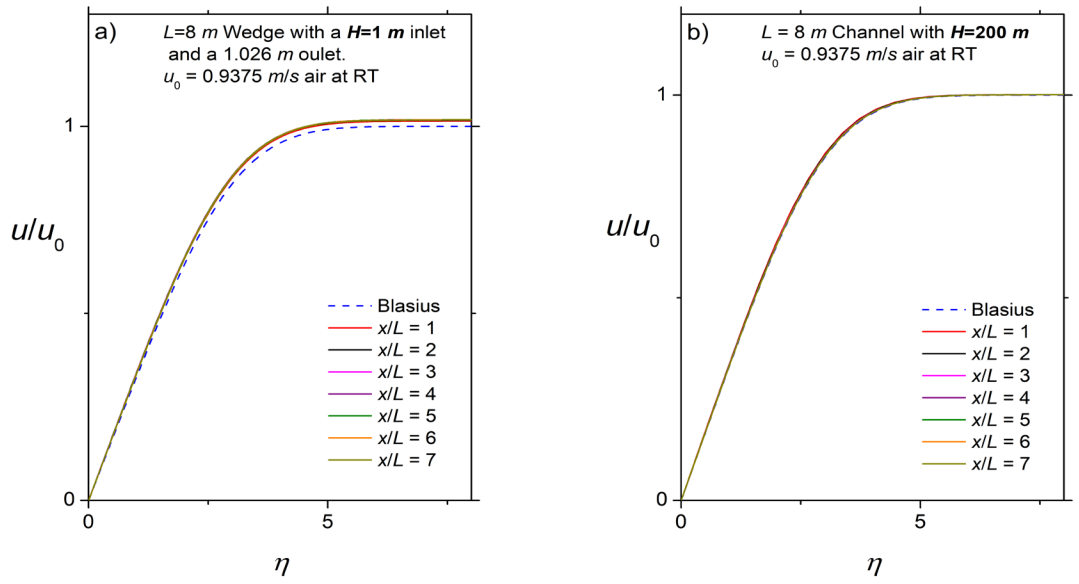

Figure 14: The Scaled *u*(*x*,*y*) Velocity Profiles for the 1-meter 2-D Wedge (a) and (b) The Scaled *u*(*x*,*y*) Velocity Profiles for the 200-meter 2-D Channel

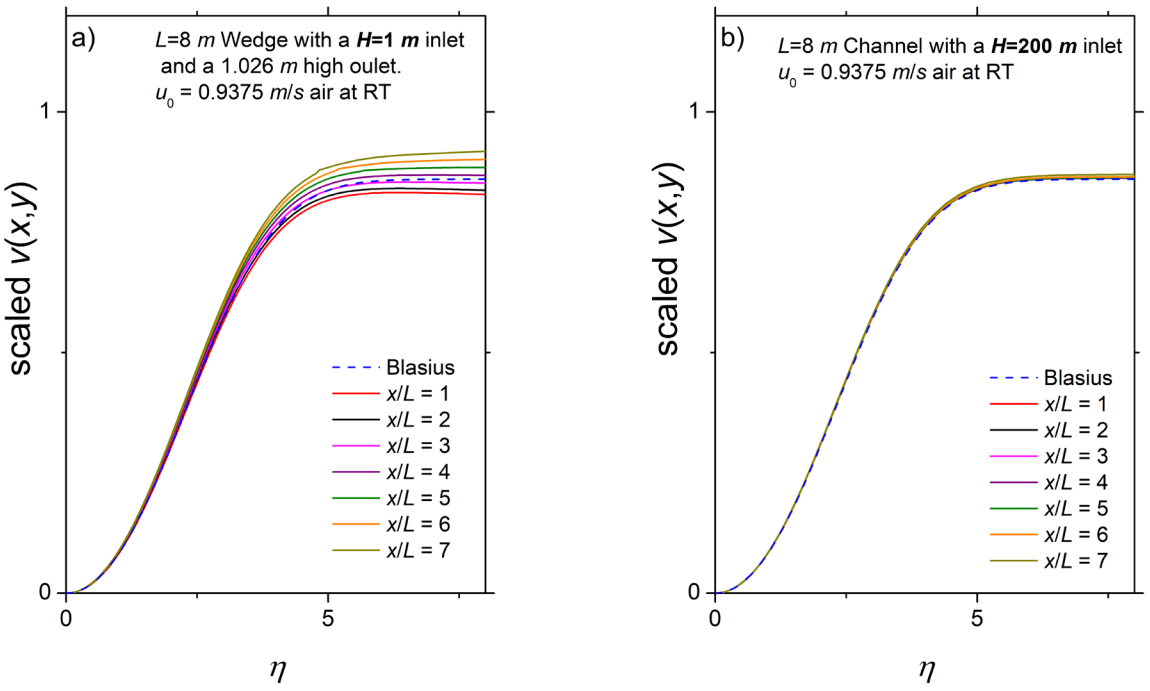

Figure 15: The Scaled *v*(*x*,*y*) Velocity Profiles for the 1-meter 2-D Wedge (a) and The Scaled v(*x*,*y*) Velocity Profiles for the 200-meter 2-D Channel

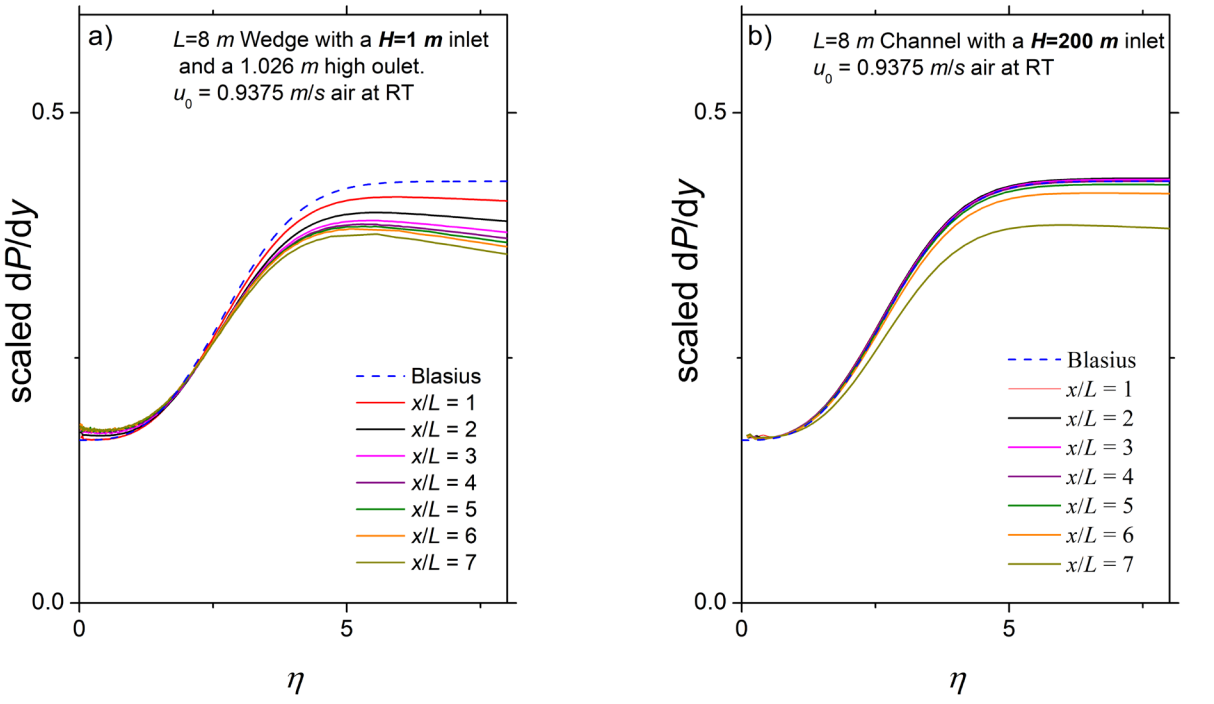

Figure 16: The Scaled *y*-pressure Gradient Profiles for the 1-meter 2-D Wedge (a) and (b) The Scaled *y*-pressure Gradient Profiles for the 200-meter 2-D Channel

It should be pointed out that the 1-meter case result shown above is different from the Air Force Tech Report[5] result. Both are 1-meter cases that have the outlet set to 1.026-meter but in the figures above, the bottom plate is kept flat and the top plate was adjusted. In the Air Force Tech Report, both the top and bottom plates were adjusted equally to give a 1.026-meter output. In the Air Force Tech Report result, the normal velocities and the normal pressure gradients also showed the same type of result showed above in Figures 14-16; the wind-tunnel-like flow does **not** correspond to Blasius similarity flow. While the Blasius flow conclusions are the same for the two cases, a significant difference is that the normal velocities shown above are positive whereas for the equal wedge angle case, the normal velocities are negative. This difference reinforces the observation that it is possible that these normal velocity variations could have effects on certain stability and transition experiments.

4. THE NORMAL TO THE WALL MOMENTUM EQUATION

In this Chapter, the theoretical description of forced laminar flow over a flat plate is revisited. In many texts, an order of magnitude argument is used to claim that the momentum equation normal to the wall reduces to just the normal pressure gradient term equal to zero. This is not a correct statement of conservation of momentum. The normal velocity must be nonzero for boundary layer flow. Hence, the normal pressure gradient cannot be zero. In what follows, a stream function analysis developed by Weyburne[16] is used to discern the true nature of the normal to the wall momentum conservation equation. The Falkner-Skan solution obtained from the x-momentum equation (parallel to the wall) is used to calculate the normal to the wall y-pressure gradient using the y-momentum equation. The y-pressure gradient for the Blasius,[6] as well as a more general Falkner-Skan solution,[17] can be obtained in this way.

For certain isothermal steady laminar flows over a flat plate, the velocity in the flow direction, $u(x,y)$, and the normal velocity, $v(x,y)$, close to the wall can be calculated using just the x-momentum equation and the mass conservation equation. This is the route taken by Blasius[6] and Falkner and Skan.[17] With the velocity solution in hand, the thinking has been that there is little need for the y-momentum equation. This has led many to actually try to dismiss the y-momentum equation entirely. It is very common to find texts indicating that the y-momentum equation reduces to just the y-pressure gradient term equal to zero (see, for example, White[18] or Cengel and Cimbala[19]). That is, many claim that the y-momentum equation reduces to

$$\frac{\partial P}{\partial y} = 0 \quad . \tag{1}$$

However, this equation is not a correct statement of momentum conservation. The boundary layers y-momentum may be small compared to the x-momentum but it definitely exists since the normal velocity $v(x,y)$ must be nonzero. Momentum must still be conserved. To state that the y-momentum for the boundary layer situation reduces to the above equation is simply wrong.

What has been lost in this widespread dismissal of the y-momentum equation is an understanding of the nature of the pressure gradient in the y-direction. When fast-moving inlet flow encounters slow moving boundary layer flow, a pressure imbalance is created in the boundary layer region. The slow-moving flow close to the wall induces a normal flow (y-direction) away from the wall due to the pressure gradient formed by this slow flow - fast flow imbalance. Weyburne[16] pointed out that the y-momentum equation provides the means to determine the pressure gradient in the y-direction once the x-momentum equation has been solved.

A simple way to explore the nature of the y-pressure gradient is to use a Falkner-Skan stream function analysis which describes laminar flow along a wall due to a pressure gradient in the flow direction. The Falkner-Skan formulation is often identified with flow along a wedge since the inertial flow just above the boundary layer edge looks similar to the pure inertial flow past a displacement thickness broadened wedge. What is not widely appreciated is that the same Prandtl x-momentum equation used by Falkner-Skan is also used to describe laminar flow along a flat plate that has a pressure gradient in the flow direction. The fast-moving free stream flow running into the slow-moving flow close to the wall induces a pressure imbalance along the wall

which takes the form of x and y pressure gradients. Flow along the inside wall of a parallel wall channel is often incorrectly associated with Blasius ZPG flow when, in fact, the pressure gradient under this condition is significantly non-zero (see Fig. 2.6b). The non-zero pressure gradient type of flow was first studied theoretically using the method developed by V. M. Falkner and Sylvia Skan in 1930.[17] Falkner-Skan developed similarity solutions to the Prandtl momentum equations for this boundary layer flow situation. The Falkner-Skan[17] analysis is outlined in most textbooks and in numerous online sites. However, those discussions are fragmented and incomplete. As such, in what follows, the relevant equations are outlined.

The Falkner-Skan analysis is best understood using a stream function approach. Underlying the Falkner-Skan stream function approach is a critical assumption to the whole theoretical development and that is that the velocities $u(x,y)$ and $v(x,y)$ can be decomposed into a product of a length and velocity x-dependent functional times and a scaled y-functional. Assume that a stream function $\psi(x,y)$ exists (see Panton,[20] p.543) such that

$$\frac{\psi(x,y)}{\delta_s(x)u_s(x)} = f(\eta) \quad , \tag{2}$$

where $f(\eta)$ is a dimensionless function that only depends on the scaled y-position ($\eta = y/\delta_s(x)$), where $\delta_s(x)$ is the length scaling parameter, and where $u_s(x)$ is the velocity scaling parameter. The stream function must satisfy the conditions

$$u(x,y) = \frac{\partial\psi(x,y)}{\partial y}, \quad \text{and} \quad v(x,y) = -\frac{\partial\psi(x,y)}{\partial x} \quad . \tag{3}$$

Falkner-Skan[17] found solutions to the x-momentum equation by assuming the scaling parameters are simple power functions of x. Recently, Weyburne[21] proved if similarity is present in a set of velocity profiles, then the length scaling parameter $\delta_s(x)$ must the displacement thickness $\delta_1(x)$ and the velocity scaling parameter $u_s(x)$ must be the boundary layer edge velocity $u_e(x)$. This holds for all 2-D boundary layer flow (see Similarity Chapter). Thus, assume that $\delta_s(x)$ and $u_s(x)$, or in this case, $\delta_1(x)$ and $u_e(x)$, are well approximated as

$$\delta_s(x) = \delta_1(x) = b(x-x_0)^n \quad \text{and} \quad u_s(x) = u_e(x) = a(x-x_0)^m \quad , \tag{4}$$

where x_0, a, b, m, and n are constants.

Combining Eqs. 4.2 and 4.3 means that the Prandtl x-momentum equation can be put into nondimensional form as

$$f''' + \alpha ff'' + \beta\left(1 - f'^2\right) = 0 \quad , \tag{5}$$

where α and β are simple functions of $\delta_s(x)$ and $u_s(x)$, or in this case $\delta_1(x)$ and $u_e(x)$. This is the Falkner-Skan x-momentum equation. It is easily verified that α and β terms become constants when $m+2n-1=0$ which means α and β reduce to

$$\beta = \frac{ab^2}{\nu} m \quad \text{, and} \quad \alpha = \frac{ab^2}{\nu}\left(\frac{1+m}{2}\right) \quad . \tag{6}$$

The normal approach is to solve Eq. 4.5 with

$$\frac{ab^2}{\nu} \quad \Rightarrow \quad 1 \quad , \tag{7}$$

which means *x*-component of the momentum balance (Eq. 4.5) becomes

$$f_1''' + \frac{m+1}{2} f_1 f_1'' + m\left(1 - f_1'^2\right) \quad = \quad 0 \quad . \tag{8}$$

Programs to solve this version of the Falkner-Skan equation are widely available. Once this equation has been solved for f_1 as a function of η_1, then one can recover the true η, f, f', and f'' by noting

$$\eta = \eta_1\sqrt{\frac{ab^2}{\nu}}, \quad f = f_1\sqrt{\frac{ab^2}{\nu}}, \quad f' = f_1', \quad \text{and} \quad f'' = f_1''\Big/\sqrt{\frac{ab^2}{\nu}} \quad , \tag{9}$$

and where f''' is recovered using Eq. 4.5. With $f(\eta)$ and its derivatives as a function of η for a given α and β, it is a simple matter to back out $u(x,y)$ and $v(x,y)$.

Weyburne[16] pointed out that with the velocities in hand, one can use these calculated velocities in the Prandtl *y*-momentum equation to obtain the *y*-pressure gradient. The Prandtl y-momentum equation for laminar flow is

$$u(x,y)\frac{\partial v(x,y)}{\partial x} + v(x,y)\frac{\partial v(x,y)}{\partial y} \quad = \quad -\frac{1}{\rho}\frac{\partial P}{\partial y} + \nu\frac{\partial^2 v(x,y)}{\partial y^2} \quad , \tag{10}$$

Substituting in the Falkner-Skan stream function result from Eq. 4.2 into Eq. 4.10, the full Falkner-Skan version of the reduced *y*-momentum equation is given by

$$\begin{aligned} \frac{(x-x_0)^2}{u_e^2\delta_1}\frac{1}{\rho}\frac{dP}{dy} \quad = \quad & -\frac{\nu}{2ab^2}(3m-1)f'' + \frac{\nu}{2ab^2}(1-m)\eta f''' - \frac{1}{4}(m+1)^2 ff' + \\ & + \frac{1}{4}(m-1)^2\eta f'^2 \quad -\frac{1}{4}(m+1)(m-1)\eta ff'' \quad . \end{aligned} \tag{11}$$

The Blasius *y*-pressure gradient version of Eq. 4,11 (corresponding to m=0 and $u_e(x)$ equal to the inlet velocity u_0) is given by

$$\frac{(x-x_0)^2}{u_0^2\delta_1(x)}\frac{1}{\rho}\frac{dP}{dy} = \frac{\nu}{2ab^2}\eta f''' + \frac{\nu}{2ab^2}f'' - \frac{1}{4}ff' + \frac{1}{4}\eta f'^2 + \frac{1}{4}\eta ff'' \quad . \tag{12}$$

The Blasius *y*-pressure gradient asymptotes at large η-values to a value of 0.4302 (one half of the normal velocity asymptote value). As η goes to zero, the scaled *y*-pressure gradient goes to 0.16603 (one half of the wall shear stress numerical value).

With *f* and its derivatives in hand, the reduced velocities and reduced pressure gradient are calculated and plotted in Figure 17. The velocities are the well-known Blasius values. For the first time, the behavior of the Blasius *y*-pressure gradient in the boundary layer is also revealed.

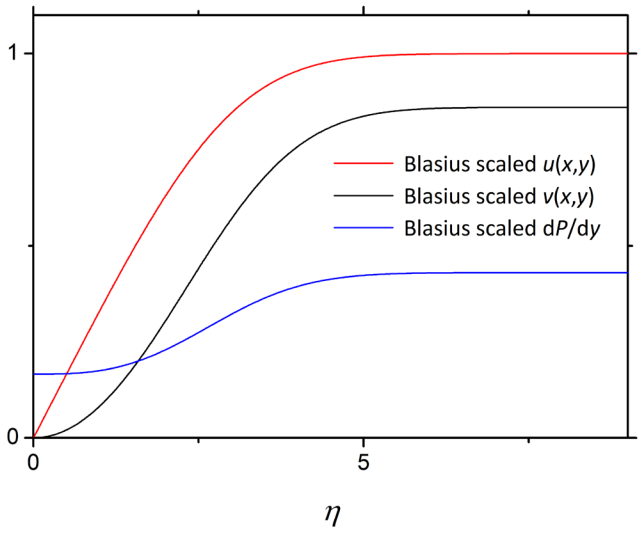

Figure 17: The Scaled Velocities and y-pressure Gradient for Blasius Flow

For the case where *m* is non-zero, Weyburne[16] presented example plots for various *m*-valued Falkner-Skan solutions.

4 BOUNDARY LAYER THICKNESS AND SHAPE

In the following, an integral moment method[22,7,8] is outlined for describing the thickness and shape of the velocity, temperature, and pressure profiles formed by fluid flow along a wall. The velocity and thermal profile moments are outlined below. The most important results of this new integral moment approach are:

- A mathematically well-defined measure of the boundary layer thickness that utilizes the entire profile, not just a few tail region data points.

- Four new parameters that help describe the thickness and shape of the boundary layer. These four parameters are the mean location, the boundary layer width, the velocity profile skewness, and the velocity profile excess. The skewness and excess are true shape parameters as opposed to the made-up parameters like H_{12}.

- Applying the moment method to the first and second derivatives of the velocity profile generates additional parameters that, for example, determines the location, shape, and thickness of the viscous forces in a turbulent boundary layer.

- It is possible to prove that many of these velocity thickness parameters are also similarity scaling parameters. That is, if similarity is present in a set of velocity profiles, then these thickness parameters must also be similarity length scaling parameters.

To begin, the velocity profile moment method[22,7,8] is outlined. What is new herein is that the moment method is specifically adopted to the "bounded" and "unbounded" boundary layer concept discussed in the first Section. Following the velocity profile section, the thermal profile moment method is outlined. The pressure and pressure gradient profiles are not covered in this review but can be deduced from the velocity and thermal profile methods.

4.1 Describing the Velocity Boundary Layer formed by Fluid Flow along a Wall

Steady 2-D fluid flowing along an interior wall with velocity $u(x,y)$ is depicted in Figure 2. Prandtl[1] observed that the velocity at the wall will be zero due to friction but then increases to an asymptotic velocity over a relatively small distance above the wall. This "boundary layer" causes drag and has significant implications on moving fluids along walls. Characterizing the thickness and shape of the velocity profile formed due to this boundary layer flow is therefore important from both a practical as well as scientific stand point. For 2-D flow, the velocity profile at a point x is defined as the velocity above the wall, $u(x,y)$, for all y. The thickness of the velocity profile is considered to be the point where the velocity just reaches the boundary layer edge velocity given by $u_e(x)$.

4.1.1 The Traditional Method

The traditional method for describing the thickness and shape of the velocity profile along a wall are rather crude and problematic. The integral based displacement thickness and the momentum thickness are certainly easily calculated but neither one describes the outer edge boundary layer thickness. As a consequence, the 99% boundary layer thickness parameter, δ_{99}, has become the

de facto standard measure. However, this parameter has problems. Since the actual mathematical form of the transition to the free stream for laminar and turbulent flow is unknown, then it is not possible to fit for δ_{99}. To determine δ_{99} from experimental data one has to interpolate using a few noisy data points. Then there is the problem for external flows. **As we saw in Figure 8, δ_{99} is totally inadequate to describe the unbounded external boundary layer thickness.** However, the most serious problem may be theoretical. There is very little chance that a theoretical derivation will prove δ_{99} is a similarity scaling thickness parameter. The traditional method to describe the shape of the boundary layer also has limitations. The usual method is to calculate the shape parameter H_{12}, which is the ratio of the displacement thickness to the momentum thickness. This is not a shape parameter in any normal physical or mathematical sense but it was the only parameter available to early practitioners that was able to discriminate between laminar and turbulent boundary layers.

4.1.2 The Moment Method for Bounded Interior Flows

There is a better way to describe the thickness and shape of the fluid boundary layer. A relatively new method[22,7,8] for describing the thickness and shape of the 2-D boundary layer utilizes the integral moment method commonly used to describe a random variable's probability distribution. The moment method for boundary layer flows was developed from the observation that the plot of the second derivative of the Blasius[6] boundary layer for 2-D laminar flow over a flat plate looks very much like a Gaussian distribution curve.[22] In Figure 18a, the Blasius second derivative profile is plotted and compared to a Gaussian curve. There are no adjustable parameters; the Gaussian curve uses the mean location and boundary layer width values (defined below) from the Blasius curve. Also shown is Figure 18b which is the velocity profile[22] obtained by twice integrating the Gaussian function compared to the Blasius velocity profile.

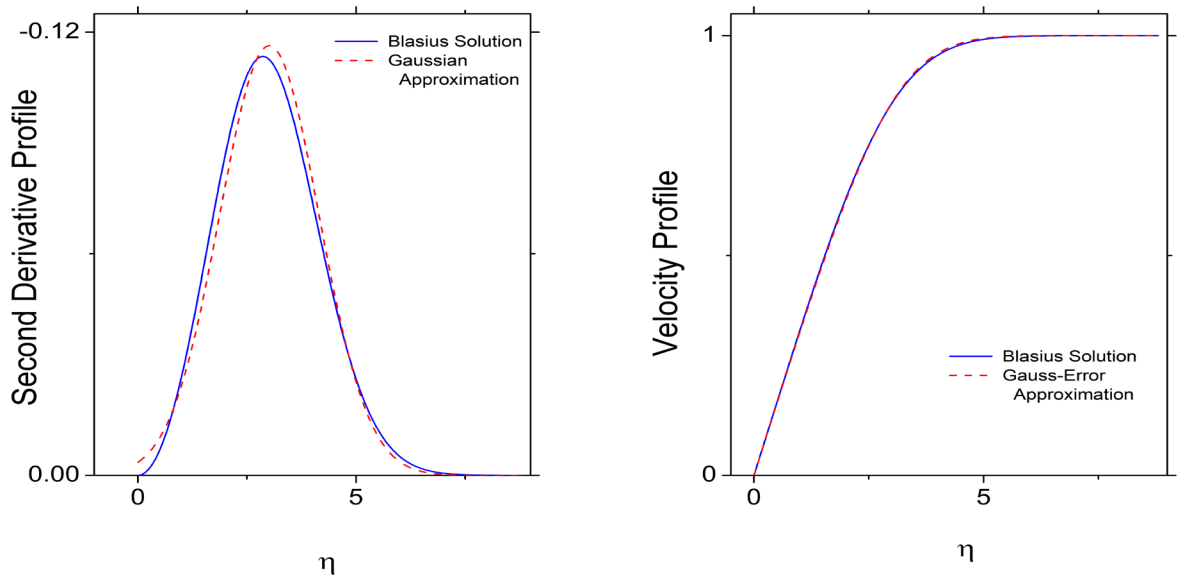

Figure 18: The Blasius Second Derivative Profile compared to a Gaussian Curve (a) and (b) the Blasius Velocity Profile compared to the Twice Integrated Gaussian Curve

It was this Gaussian-like appearance that prompted the idea of adapting the mathematics to describe probability distribution function technology to boundary layers. Weyburne started with the second derivative description but soon applied it to the velocity profile and first derivative profile.[7,8] It is straightforward to cast the properly scaled velocity profile and its first two derivatives into probability-distribution-like integral kernels with the zeroth central moment set normalized to one. It will also work for the temperature profiles and the pressure profiles.

As a demonstration, the moment method is applied to a 2-D channel with height H. Fluid flowing along the inside walls has velocity $u(x,y)$, where x is the flow direction, and y is the normal to the plate. Assume the height H is much thicker than the maximum viscous boundary layer thickness. The velocity profile's probability-distribution-like central moments for 2-D interior flows are defined in terms of moments of $1\text{-}u(x,y)/u_e(x)$. Thus, the velocity boundary layer nth moment $\zeta_n(x)$ is defined as

$$\zeta_n(x) = \int_0^{H/2} dy \left(y - m(x)\right)^n \frac{1}{\delta_1(x)}\left(1 - \frac{u(x,y)}{u_e(x)}\right) , \tag{13}$$

such that the displacement thickness $\delta_1(x)$ insures $\zeta_0(x)$ is normalized to one. The mean location of the velocity profile, $m(x)$, is formally defined as the first y-moment about zero and is given by

$$m(x) = \int_0^{H/2} dy\, y \frac{1}{\delta_1(x)}\left(1 - \frac{u(x,y)}{u_e(x)}\right) , \tag{14}$$

where the displacement thickness, $\delta_1(x)$, is defined as

$$\delta_1(x) = \int_0^{H/2} dy \left(1 - \frac{u(x,y)}{u_e(x)}\right) . \tag{15}$$

As discussed in the papers, there are some advantages to also calculating the integral moments of the derivatives of the velocity profile. The first derivative nth central moment, $\kappa_n(x)$, is defined as

$$\kappa_n(x) = \int_0^{H/2} dy \left(y - \delta_1(x)\right)^n \frac{d\left\{u(x,y)/u_e(x)\right\}}{dy} , \tag{16}$$

so that $\kappa_0(x)$ normalizes to one. The mean location of the derivative of the stream-wise velocity profile is formally defined as the first y-moment about zero and, in this case, is just the displacement thickness, $\delta_1(x)$.

The viscous second derivative velocity boundary layers *n*th central moment, $\lambda_n(x)$ is defined as

$$\lambda_n(x) = \int_0^{H/2} dy \left(y-\mu_1(x)\right)^n \frac{d^2\left\{-\mu_1(x)\,u(x,y)/u_e(x)\right\}}{dy^2} \quad , \tag{17}$$

where the mean location is the first moment about zero, $\mu_1(x)$, and is obtained from the requirement that the zeroth moment, $\lambda_0(x)$, have a value of unity. Thus, the mean location of the boundary layer $\mu_1(x)$ is given by

$$\frac{u_e(x)}{\mu_1(x)} = \left.\frac{du(x,y)}{dy}\right|_{y=0} \Rightarrow \mu_1(x) = \frac{\upsilon u_e(x)}{\tau_w} \quad , \tag{18}$$

where υ is the viscosity. This means $\mu_1(x)$ is inversely proportional to the wall shear stress, τ_w.

With the moments and the mean locations defined, the boundary layer thickness and shape can be described in terms of the boundary layer mean locations, widths (variance), skewnesses, and excesses (excess kurtosis). Experimentally, it is found[8] that the turbulent boundary layer thickness defined as $\delta_s = \delta_1+3\sigma_s$ (where $\sigma_s = (\kappa_2)^{1/2}$) tracks the 99% thickness very well.

Taking a cue from the boundary layer momentum balance equations, the second derivative boundary layer moments, λ_n, track the thickness and shape of that portion of the boundary layer where the viscous forces are significant. Weyburne[7,8] showed that the viscous thickness, given by $\delta_v(x) = \mu_1(x) +2\sigma_v$ (where $\sigma_v = (\lambda_2)^{1/2}$) approximately tracks the 99% thickness for laminar flow. For turbulent flows, the moment method makes it possible to track and quantify the inner viscous region using λ_n moments whereas the outer region of the turbulent boundary layer can be tracked using ζ_n and κ_n moments.

Calculation of the derivative moments without the need to differentiate the u(x,y) profile is simplified by using integration by parts to reduce the moments to simply integrals based on the displacement thickness kernel. Thus, if

$$\alpha_n(x) = \int_0^{H/2} dy\, y^n \left(1-\frac{u(x,y)}{u_e(x)}\right) \quad , \tag{19}$$

then the first derivative skewness, for example, can be calculated as

$$\gamma_1(x) = \frac{\kappa_3(x)}{\kappa_2^{3/2}(x)} = \frac{2\delta_1^3(x)-6\delta_1(x)\alpha_1(x)+3\alpha_2(x)}{\left(-\delta_1^2(x)+2\alpha_1(x)\right)^{3/2}} \quad . \tag{20}$$

This parameter was shown[7,8] to track the boundary layer shape changes that accompany the laminar to turbulent boundary layer transition.

4.1.3 The Moment Method for Unbounded Flows

For exterior flows, there are a number of ways to modify the above equations to make new moment expressions correctly describe the thickness and shape of the exterior boundary layer. One version (see Weyburne[3-5]) is to divide the boundary layer into two regions around the maximum velocity u_{max}. For the region between the wall and the u_{max} location, the above equations can be used but with u_{max} replacing $u_e(x)$ and δ_{max} replacing $H/2$. For the part of the boundary layer between the u_{max} location and deep into the free stream, the inertial moments described in the Air Force Tech Report[3] are preferred.

Numerical errors encountered in calculating the moments, especially the higher order moments, is a serious concern. **In all cases, the numerical calculation recommendations mentioned in the earlier papers[7,8] should be followed to avoid these errors.**

4.1.4 The Moment Method Problem Area

There are instances where the moment method has problems for certain types of velocity profiles. For example, when an interior flow has an adverse pressure gradient in the flow direction, the second derivative of the velocity can take on negative values in the near wall region. Negative values are not allowed in standard probability framework so the application of the moment methodology will result in biased measures for this case. Weyburne[3] pointed out a fix is to simply exclude the negative values and define a new set of moments for a truncated second derivative profile starting at the second derivative maximum. This fix will then properly identify the thickness location where the second derivative profile becomes negligible above the wall.

4.1.5 The Moment Thickness Parameters as Similarity Scaling Parameters

One of the advantages of the new thickness parameters is that certain of these parameters are also similarity length scaling parameters if velocity profile similarity is present along the wall. For 2-D wall-bounded flows, velocity profile similarity is defined as the case where two velocity profiles taken at different stations along the flow differ only by simple scaling parameters in y and $u(x,y)$. Weyburne[23] has presented theoretical proof that some of the above moment parameters, including δ_1, μ_1, and σ_s are similarity length scaling parameters. That is, if similarity is discovered in a set of 2-D velocity profiles, then δ_1, μ_1, and σ_s must be similarity length (height) scaling parameters.

It is also worth noting that the new second derivative mean thickness $\mu_1(x)$ will actually perform similarly to the Prandtl Plus scaling's for similarity scaling of the inner wall region of experimental data sets. If a set of velocity profiles is plotted on a graph using $\mu_1(x)$ and $u_e(x)$ as the thickness and velocity scaling parameters and then compared to plots using the Prandtl Plus scaling parameters, the plots will look identical if the Rotta constraint holds ($u_\tau(x)/ u_e(x)$ = constant). The key to this is realizing that multiplying both the Prandtl scaling variables by the factor u_e/u_τ results in the $\mu_1(x)$ and $u_e(x)$ scaling parameters (see Eq. 18). Hence, the relative relationships between the plotted curves for the two parameter sets will appear identical if the Rotta constraint holds.

4.2 Describing the Thermal Boundary Layer formed by Fluid Flow along a Wall

Weyburne[22] showed that the second derivative of the scaled temperature profile also shows Gaussian-like behavior. Hence, the same moment method technology for describing the thickness and shape of the velocity profiles can also be used to describe the thermal boundary layer profile.[24] This "thermal boundary layer" can have a significant impact on the efficiency of heating/cooling equipment, among other things. Characterizing the thickness and shape of the thermal boundary layer is therefore important from both a practical as well as scientific stand point.

To demonstrate the new method, consider a semi-infinite 2-D channel with height H. Fluid flowing along the inside walls has velocity $u(x,y)$, where x is the flow direction, and y is the normal to the plate. Assume the height H is much thicker than the maximum velocity or temperature boundary layer thickness. Assume the fluid has a temperature $T(x,y)$, the temperature at the wall is T_w, and the free stream fluid temperature is T_0. Applying the integral moment method, the thermal boundary layer can be described in terms of the central moments, $\xi_n(x)$, given by

$$\xi_n(x) = \int_0^{H/2} dy \left(y - m_T\right)^n \frac{1}{\beta_0(x)} \frac{T(x,y) - T_0}{T_w - T_0} \quad , \tag{21}$$

where the thermal displacement thickness $\beta_0(x)$ is the normalizing constant. The first moment about zero, which is called the mean location, is defined as

$$m_T(x) = \int_0^{H/2} dy\, y \frac{1}{\beta_0(x)} \frac{T(x,y) - T_0}{T_w - T_0} \quad , \tag{22}$$

such that the thermal displacement thickness, $\beta_0(x)$, is defined as
(

$$\beta_0(x) = \int_0^{H/2} dy \frac{T(x,y) - T_0}{T_w - T_0} \quad . \tag{23}$$

As discussed in the papers, there are some advantages to also calculating the integral moments of the derivatives of the thermal profile. Let

$$\theta(x,y) = \frac{T(x,y) - T_0}{T_w - T_0} \quad , \tag{24}$$

then the thermal first derivative central moments, $\varepsilon_n(x)$, are defined as

$$\varepsilon_n(x) = -\int_0^{H/2} dy \left(y - \beta_0(x)\right)^n \frac{d\theta(x,y)}{dy} \quad , \tag{25}$$

where the thermal displacement thickness $\beta_0(x)$ (Eq. 23) is the mean location.

The thermal second derivative central moments, $\chi_n(x)$, are defined as

$$\chi_n(x) = \int_0^{H/2} dy \left(y - \mu_T(x)\right)^n \frac{d^2\left\{\mu_T(x)\theta(x,y)\right\}}{dy^2} \quad , \tag{26}$$

where, $\mu_T(x)$ is both the normalizing constant and also happens to be the second derivatives mean location. The mean location, $\mu_T(x)$, is formally defined as the first y-moment about zero but is actually defined by requiring $\chi_0(x)$ to be normalized to one. Thus,

$$\chi_0(x) = 1 = \int_0^{H/2} dy \frac{d^2\left\{\mu_T(x)\theta(x,y)\right\}}{dy^2} \Rightarrow \frac{1}{\mu_T(x)} = -\frac{d\theta(x,y)}{dy}\bigg|_{y=0} \quad . \tag{27}$$

With the moments and the thermal mean location defined, the thermal boundary layer thickness and shape can be described in terms of the thermal boundary layer width (variance), σ_T, the thermal skewness, and thermal excess (excess kurtosis). For the Pohlhausen[25] solution for laminar flow on a heated flat plate, it is found that thermal boundary layer thickness defined as $\delta_T = m_T(x) + 4\sigma_T$ where $\sigma_T = (\xi_2)^{1/2}$, tracks the 99% thickness very well.[24]

For laminar flow, the three different moment cases all give similar values for the thermal boundary layer thickness. For turbulent flow, the thermal boundary layer can be divided into a region near the wall where thermal diffusion is important and an outer region where thermal diffusion effects are mostly absent. **Taking a cue from the boundary layer energy balance equation, the second derivative boundary layer moments, χ_n, track the thickness and shape of that portion of the** thermal boundary layer **where thermal diffusivity, α, significant.** Hence the moment method makes it possible to track and quantify the region where thermal diffusivity is important using χ_n moments whereas the overall thermal boundary layer is tracked using ε_n and ξ_n moments. Calculation of the derivative moments without the need to take derivatives is simplified by using integration by parts to reduce the moments to simply integrals based on the thermal displacement thickness kernel auxiliary integrals.[24]

The above development applies to bounded interior flows. The equivalent development for unbounded exterior flows has not been formally presented. There does not appear to be a reason the same trick of dividing the boundary layer into two regions should not work. This would involve an inner region where thermal diffusivity, α, is significant and an outer region where thermal diffusivity is not significant.

5 BOUNDARY LAYER SIMILARITY

One of the fundamental notions in fluid mechanics is to analyze experimental observables using dimensional analysis with the intent of finding scaling parameters that render the scaled observable from different stations along the flow to appear to be similar. Similarity of the velocity profile formed by fluid flow along a wall is one of those fundamental notions. For 2-D wall-bounded flows, velocity profile similarity is defined as the case where two velocity profiles taken at different stations along the flow differ only by simple scaling parameters in y and $u(x,y)$, where y is the normal direction to the wall, x is the flow direction, and $u(x,y)$ is the velocity parallel to the wall in the flow direction. One of the keys to any similarity solution is identifying the correct scaling parameters. In the following, a proof developed by Weyburne[21] is outlined that, **for similarity to be present in any 2-D fluid boundary layer, the length scaling parameter must be the displacement thickness $\delta_1(x)$ and the velocity must be the velocity at the boundary layer edge $u_e(x)$.**

5.1 Similarity of the Boundary Layers Velocity Profile

Although fluid flow can be described theoretically using the well-known Navier–Stokes governing equations, there are few analytical solutions to this set of partial differential equations. Furthermore, the computer-based solutions for most flow situations are very time consuming even with very fast computers. Fortunately, under certain flow conditions, the flow downstream can look geometrically similar to the upstream flow, differing only by simple scaling parameters. When this happens, the set of partial differential flow governing equations can be simplified to an easily solved set of ordinary differential equation. The "similarity" solution for boundary layer flows represent one of these known solution sets. These similarity solutions provide valuable insights into the physics governing the fluid flow in the boundary layer.

Traditionally, the theoretical study of similarity of boundary layer flows involved the mathematical aspects of solutions to the Navier-Stokes equation. Recently, Weyburne[21] described a way to actually determine the identity of the similarity parameters for boundary layer flows. The approach is based on a simple concept; the area under a set of scaled velocity profile curves that show similarity behavior must be equal. This led to a new integral-based derivation that proved that if similarity is present in a set of velocity profiles, then the similarity velocity scaling parameter must be the velocity at the boundary layer edge $u_e(x)$ and the similarity length scaling parameter must be the traditional displacement thickness, $\delta_1(x)$. **This proof works for the bounded boundary layer case where the flow asymptotes to $u_e(x)$.** For the unbounded boundary layer case, Weyburne[5] extended the argument to the exterior flow, unbounded boundary layer case where the velocity peaks before asymptoting to the free stream velocity u_0.

5.1.1 Similarity of the Bounded Boundary Layer

T demonstrate the proof, we consider the "bounded" boundary case for interior flows. Assume a steady boundary layer flow develops along an interior 2-D channel wall with velocity $u(x,y)$, where y is the normal direction to the wall, x is the flow and wall direction. The velocity profile is defined as the velocity above the wall $u(x,y)$ for all y at a fixed x position. The velocity profile is assumed to smoothly asymptote to the boundary layer edge velocity $u_e(x)$. The channel width

H is assumed to be much thicker than the maximum boundary layer thickness found in the channel but not so thick that unbounded boundary layer conditions are present.

Assume a set of scaled profiles is found that show similarity when scaled with the as yet unidentified velocity scaling parameter $u_s(x)$ and the unidentified thickness scaling parameter $\delta_s(x)$. According to Schlichting,[2] boundary layer similarity is then defined as the case where the scaled velocity profile at a station x_1 is similar to the scaled profile at x_2 if

$$\frac{u\left(x_1, y/\delta_s(x_1)\right)}{u_s(x_1)} = \frac{u\left(x_2, y/\delta_s(x_2)\right)}{u_s(x_2)} \quad \textit{for all } y. \tag{28}$$

The velocity $u(x,y)$ is written in this way to specify that the scaled velocity profile thickness comparisons are made at the equivalent $y/\delta_s(x)$ values and not at the equivalent y-values.

Rather than starting with velocity profile similarity, consider the derivative of the velocity profile since this result will be needed for the next step. **Similarity necessarily requires that if the scaled profiles are similar, then the scaled derivatives of the velocity profiles must also be similar.** This, in turn, means that the scaled derivative profiles plotted versus the similarity scaled y-value must all have equal areas under the scaled derivative curves. In mathematical terms, the area under the scaled first derivative profile curve is expressed by

$$a(x) = \int_0^{h/\delta_s} d\left\{\frac{y}{\delta_s}\right\} \frac{d\left\{u(x, y/\delta_s)/u_s\right\}}{d\left\{\frac{y}{\delta_s}\right\}} \quad , \tag{29}$$

where a(x) will be, in general, a non-zero numerical constant as long as y=h is deep into the free stream above the wall but less than H/2. For clarity, h(x), u_s(x), and δ_s(x) have been shortened to h, u_s, and δ_s. **Assuming the boundary conditions u(x,0)=0 and u(x,h)=u_e(x),** and, using a simple variable switch, Eq. 29 can be shown to reduce to

$$a(x) = \frac{u_e(x)}{u_s(x)} \quad . \tag{30}$$

Similarity requires that $a(x_1)=a(x_2)$. Similarity also requires that $h(x_1)/\delta_s(x_1) = h(x_2)/\delta_s(x_2)$ but this is easily satisfied as long as $h(x_1)$ and $h(x_2)$ are chosen appropriately and are located deep into the free stream. Since $u_s(x)$ is a similarity parameter, this result necessarily requires that if similarity is present in a set of velocity profiles in the near wall region, then $u_e(x)$ must also be a similarity velocity scaling parameter.

This same result is also obtained from the definition equation for similarity, Eq. 28, by taking the limit y going deep into the free stream. In addition, previous theoretical studies by Rotta,[26] Towsend,[27] Castillo and George,[28] and Kitsois, *et. al.*[29] have all identified $u_e(x)$ as a similarity scaling parameter. Yet, there is extensive literature that has dealt with the search for **other** velocity scaling parameters for 2-D turbulent boundary layer flows. They propose other velocity scaling

parameters as being somehow superior to $u_e(x)$ **without** ever explaining why all of these different theoretical approaches that have identified $u_e(x)$ as a similarity scaling parameter are faulty. The problem with this flawed thinking is detailed in the Chapter 7. **In any case, unless one changes the definition of similarity or the velocity boundary conditions, the velocity at the boundary layer edge $u_e(x)$ must be the velocity similarity scaling parameter.**

Next, consider the area under the velocity profile curves. Starting with the formal definition of similarity given by Eq. 31 then it is self-evident that for the profiles to be similar, the area under these scaled velocity profiles plotted versus the scaled y-coordinate must be equal. The area under the scaled profiles, in mathematical terms, is given by

$$b(x) = \int_0^{h/\delta_s} d\left\{\frac{y}{\delta_s}\right\} \frac{u_e - u(x, y/\delta_s)}{u_s} \quad , \tag{31}$$

where $b(x)$ will, in general, be a nonzero numerical constant, and where the velocity is written in terms of the defect profile $u_e(x)$-$u(x,y)$. **Using the result from Eq. 30, it is easily verified that similarity requires that $b(x_1)=b(x_2)$.** By employing a simple variable switch, Eq. 31 can be shown to reduce to

$$b(x) = \frac{\delta_1(x)\, u_e(x)}{\delta_s(x)\, u_s(x)} \quad , \tag{32}$$

by recognizing that the displacement thickness, $\delta_1(x)$, is defined as

$$\delta_1(x) = \int_0^h dy \left\{1 - \frac{u(x,y)}{u_e(x)}\right\} \quad . \tag{33}$$

Since similarity requires that $b(x_1)=b(x_2)$, then, combining with the Eq. 30 result, this result necessarily means that **if similarity is present in a set of velocity profiles, then the displacement thickness $\delta_1(x)$ must be a similarity length scaling parameter**. This result applies to **all** bounded 2-D fluid flows along a flat plate.

The net result is that if similarity is present in a set of 2-D bounded velocity profiles, then the length scale must be the displacement thickness $\delta_1(x)$ and the velocity scale must be $u_e(x)$. **The results are mathematically rigorous; they are only dependent on the definition of similarity, the definition of the displacement thickness, and the boundary conditions.** Interestingly, $\delta_1(x)$ is not the only integral moment parameter that works. Weyburne[23] pointed out that other moment method thickness parameters, such as $\mu_1(x)$ (see Eqs. 17 and 18), are also similarity scaling parameters.

5.1.2 Similarity of the Unbounded Boundary Layer

Weyburne[5] extended the same type of argument to the 2-D laminar flow unbounded boundary layer case. For the unbounded boundary layer case, the boundary layer is divided into two

regions, the viscous-like inner region and the inertial-like outer region. The dividing location can be conveniently chosen to be δ_{max}, the location of the maximum velocity u_{max}. It was demonstrated that the viscous region showed similarity when scaled with the "maximum displacement thickness", $\delta_1^m(x)$, given by

$$\delta_1^m(x) = \int_0^{\delta_{max}} dy \left\{ \frac{u_{max} - u(x,y)}{u_{max}} \right\} , \tag{34}$$

is the length scale and the velocity scaling parameter is u_{max} (see Weyburne[5] for the details). It should also be mentioned that Weyburne[3] speculated that the inertial boundary layer region for unbounded laminar flows might display similar behavior. However, it was subsequently found that this was not true for unbounded laminar flow along a flat plate.[5]

5.2 Similarity of the Thermal Boundary Layer Profile

The similarity of the thermal boundary layer formed by fluid flowing a long a heated or cooled wall can be handled in a similar fashion as the velocity profile similarity (see Weyburne[30]). The Navier–Stokes governing equations can be extended to include the energy balance equations. The solution to this expanded set of partial differential equations for a particular flow situation is, in general, very time consuming even with very fast computers. Under certain flow conditions, the thermal profile and the velocity profile downstream can look geometrically similar to the upstream flow, differing only by simple scaling parameters. When this happens, the set of partial differential flow governing equations can be simplified to an easily solved set of ordinary differential equation. The similarity solution for heated/cooled boundary layer flows represent one of these known solution sets.

To demonstrate the proof, we consider a boundary layer flow along the heated/cooled inside wall of a 2-D channel with gap H. The channel half width, $H/2$, is assumed to be much thicker than the maximum velocity and thermal boundary layer thickness found in the channel. Let the velocity be u(x,y) and temperature $T(x,y)$, where y is the normal direction to the wall and x is the flow direction. Assume the flow conditions discussed in Section 6.1 hold and that the channel wall is isothermal with a temperature, T_w, and the free stream is isothermal with a temperature, T_0. The temperature profile is defined as the temperature $T(x,y)$ taken at all y values starting from the wall moving outwards at a fixed x value. Temperature profile similarity is defined as the case where two temperature profile curves from different stations along the wall in the flow direction differ only by a scaling parameter in y and a scaling parameter of the temperature profile $T(x,y)$.

Assume a set of temperature profiles are found that display temperature profile similarity when scaled with the height scaling parameter $\delta_q(x)$ and the temperature scaling parameter T_s. The scaled temperature profile at a station x_1 is said to be similar to the scaled profile at x_2 if

$$\frac{T\left(x_1, y/\delta_q(x_1)\right)}{T_s(x_1)} = \frac{T\left(x_2, y/\delta_q(x_2)\right)}{T_s(x_2)} \quad \text{for all } y. \tag{35}$$

The temperature $T(x,y)$ is written in this way to specify that the scaled temperature comparisons are made at the equivalent $y/\delta_q(x)$ values and not at the equivalent y-values. An important observation about the isothermal wall is that in the limit of $y \to 0$ and $y \to H/2$, the temperature ratios in Eq. 35 both reduce to $T_w/T_s(x)$ and $T_0/T_s(x)$ which means that $T_s(x)$ must be a constant. This means that for similarity, only the length scaling parameter $\delta_q(x)$ may vary with the flow direction.

To discover the identity of T_s and $\delta_q(x)$, the same technique that was used for the velocity profile similarity method discussed above is applied. As with the velocity case, start by considering the first derivative of the temperature profile since this will be needed in the next step. **If similarity is present in a set of temperature profiles then it is self-evident that the properly scaled first derivative profile curves (derivative with respect to the scaled *y*-coordinate) must also be similar.** It is also self-evident that the area under the scaled first derivative profiles plotted against the scaled y-coordinate must be equal. In mathematical terms, the area under the scaled first derivative profile curve is given by

$$p(x) = \int_0^{h/\delta_s} d\left\{\frac{y}{\delta_s}\right\} \frac{d\left\{T\left(x, y/\delta_s\right)/T_s\right\}}{d\left\{\frac{y}{\delta_s}\right\}} \quad , \tag{36}$$

where h is deep into the free stream above the wall but less than $H/2$. Using the boundary conditions and a simple variable switch, Eq. 36 can be shown to reduce to

$$p(x) = \frac{T_0 - T_w}{T_s} \quad . \tag{37}$$

Similarity requires that $p(x_1) = p(x_2)$. Hence, the similarity scaling parameter T_s must be proportional to the temperature difference $T_0 - T_w$.

Now consider the identity of $\delta_q(x)$. Starting with the formal definition of similarity given by Eq. 35 then it is self-evident that for the profiles to be similar, the area under these scaled temperature profiles plotted versus the scaled y-coordinate must be equal. The area under the scaled temperature profile is not easily manipulated. However, Eq. 35 can be used to advantage. If a constant is added or subtracted from both sides of Eq. 35 and then integrated, the equivalence condition still holds. Subtracting $T_0/(T_0 - T_w)$ value from both sides of Eq. 35 and integrating, the area, in mathematical terms, is given by

$$r(x) = \int_0^{h/\delta_s} d\left\{\frac{y}{\delta_s}\right\} \frac{T_0 - T\left(x, y/\delta_s\right)}{T_0 - T_w} \quad , \tag{38}$$

where $r(x)$ is, in general, a nonzero numerical constant. Using a simple variable switch and simple algebra, Eq. 38 can be shown to reduce to

$$r(x) \;=\; \delta_1^T(x) \big/ \delta_q(x) \quad , \tag{39}$$

where the thermal displacement thickness $\delta_1^T(x)$ is defined as

$$\delta_1^T(x) \;=\; \int_0^h dy \; \frac{T(x,y)-T_0}{T_w-T_0} \quad . \tag{40}$$

Similarity requires that $r(x_1)=r(x_2)$. The importance of Eq. 39 in regards to similar profiles is that it means that if similarity is present in a set of thermal profiles for any 2-D boundary layer along a wall, then the **thickness scaling parameter $\delta_q(x)$ must be the thermal displacement thickness $\delta_1^T(x)$**. From Eq. 37, we showed that the similarity **temperature scaling parameter T_s must be proportional to the temperature difference $T_0 - T_w$. The results are mathematically rigorous; they are only dependent on the definition of similarity, the definition of the thermal displacement thickness, and the boundary conditions.**

Perhaps the best way to demonstrate this new result is to apply the new similarity scaling parameters to a data set from the literature. In Figure 19a the results for the Pohlhausen[25]-based approach to calculating the thermal profiles for laminar flow over a heated plate for a range of Prandtl numbers is presented. This figure is a re-creation of Fig. 12.9 from Schlichting[2] using a simple FORTRAN program to generate the solutions. In Figure 19b, the same data is plotted using the new thermal displacement thickness scaling parameter. **In this case, all nine curves are collapsed onto one another indicating thermal profile similarity is present.** This is a remarkable result that provides solid support for the integral area similarity theory. In this figure, the reduced plotting parameters are

$$\theta(x,y) \;=\; \frac{T(x,y)-T_0}{T_w-T_0} \quad \text{, and} \quad \eta \;=\; y\sqrt{\frac{u_0}{\nu x}} \quad , \tag{41}$$

where ν is the kinematic viscosity.

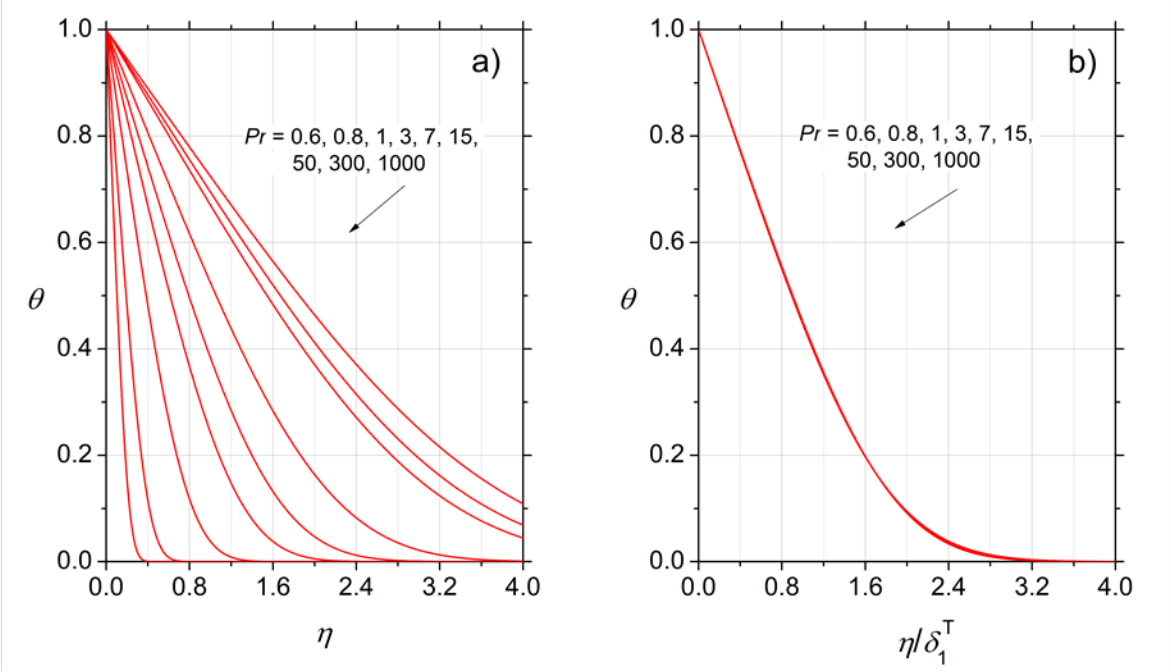

Figure 19: A Reproduction of Pohlhausen[25] Temperature Profiles from Figure 12.9 in Schlichting[2] (a) and (b)The Collapsing of Profiles from Figure 20a using the Thermal Displacement Thickness

6 TURBULENT BOUNDARY LAYER DEFECT PROFILE SIMILARITY: A CASE OF BAD SCIENCE

In this Chapter, the research work on similarity scaling for the Turbulent Boundary Layer (TBL) for the last 70 years is reviewed and found to be flawed. The work has led to the incorrect identification of the similarity scaling parameters and the mistaken belief that turbulent boundary layer similarity is common. As a remedy, the similarity scaling parameters that were identified by Weyburne[21] are tested and found to give reasonable results for certain experimental wind tunnel results. The same flawed approach is also found in the Thermal TBL literature which is briefly discussed at the end of the Chapter.

The idea of velocity profile similarity and thermal profile similarity are well known for laminar flow along a wall. For turbulent flow along a wall, it is generally acknowledged (Marusic, *et. al.*[31]) that whole profile similarity, with the exception of sink flow, has not been observed in turbulent boundary layer flows. The turbulent boundary layer has a viscous inner region and an inertial outer region so instead of looking for similarity over the whole profile, researchers started looking for similarity in just the inner or outer regions. The fact that the Navier-Stokes governing equations for turbulent flow do not have a closed form solution means that the mathematical approach to similarity used by Blasius[6] and Falkner-Skan[17] for laminar flow will not work for turbulent flows. The flow community had some early theoretical guidance beginning with the work of Rotta[26] and Towsend[27] that indicated that the velocity at the boundary layer edge, $u_e(x)$, should be a similarity velocity scaling parameter. However, this insight was largely ignored in the pursuit of "better" alternatives. **It turns out that this pursuit for better similarity parameters has been based on a false premise that negates much of the TBL similarity scaling work of the last 70 years.** In the following Chapter, the problem with the turbulent boundary layer similarity literature is outlined and discussed followed by a brief outline of a similar problem identified in the temperature profile similarity literature.

To understand the nature of this TBL similarity problem, it is necessary to go back to the work of Fredrick Clauser[32] in the 1950's. Clauser set out to explore 2-D TBL similarity of the velocity profile. He demonstrated that if he plotted a series to TBL data sets from various groups as velocity profiles, there was no similarity present. However, when he plotted the same data as **defect profiles** defined as $u_e(x)$-$u(x,y)$, where $u(x,y)$ is the velocity in the flow direction (x-direction) and $u_e(x)$ is the corresponding velocity at the boundary layer edge, then the visual inspection of the plotted data sets showed good overlap suggesting that similarity **was** present. Following closely after Clauser's work, Rotta[26] and Towsend[27] developed the **defect profile-based theory** of TBL similarity. Subsequent searches for similarity scaling parameters for the 2-D TBL have adapted the use of the defect profile as a means of "discovering" similar behavior. What followed has been 70 years of research culminating in work by Castillo and George[28] and others, that indicate that TBL similarity is widespread and occurs for most TBL data sets **if** one uses the velocity scaling parameter $u_{ZS}(x) = u_e(x)\delta_1(x)/\delta_{99}(x)$ developed by **Zagarola and Smits**.[33] Prior to the work of Castillo and George, TBL similarity of the outer region was considered rare.

All of the extensive literature concerning experimental investigations into wall-bounded TBL similarity has been based on the defect profile. To even suggest using the experimentally measured velocity profile to study similarity, as is done for laminar flows, is considered wrong and, according to some, shows a lack of understanding of turbulent boundary layer theory. However, a review of turbulent boundary layer literature reveals there has never been a theoretical justification for this defect profile preference. Therefore, the preference for the defect profile originates solely from the success of experimental comparisons; there is no theoretical preference. Stepping back and looking at the situation from a theoretical perspective, there should be **no** preference. As we will show below, theory indicates that velocity profile and defect profile similarity must occur simultaneously. This is evident when one considers that the occurrence of similarity is intimately tied to the physics of the flow. It is not possible to change the physics of the flow by simply re-plotting the data set after subtracting off the endpoint. **Simple mathematical manipulation of the data does not change the physics.**

And yet, that is exactly what appears to be happening in this case. Weyburne[34,35] recently reexamined some of these TBL data sets that others claim to show defect profile similarity and found that the defect profiles did indeed appear to show similar behavior. However, when the same data is re-plotted as standard velocity profiles, visual inspection of the plotted data sets no longer show similarity just as Clauser observed for the data sets he investigated. To understand why the appearance of similarity in one case and not the other is a problem, one can point to the argument that the simple mathematical manipulation of the data set cannot change the physics. However, the flow community has managed to ignore this simple fact for 70 years and this argument is unlikely to change anyone's thoughts today.

Therefore, to fully understand why the appearance of similarity in one case and not the other is a problem, it is useful to first review the definition of velocity profile similarity. Recall that similarity of the velocity profile for 2-D wall-bounded flows is defined as the case where two velocity profiles taken from different stations along the flow differ only by simple scaling parameters in y and $u(x,y)$. **Assume a set of velocity profiles is discovered that show similarity in the outer region when scaled with the length scaling parameter $\delta_s(x)$ and the velocity scaling parameter $u_s(x)$.** For the outer region of the TBL, the scaled velocity profile at a station x_1 along the wall will be similar to the scaled profile at x_2 when

$$\frac{u\left(x_1, y/\delta_s(x_1)\right)}{u_s(x_1)} = \frac{u\left(x_2, y/\delta_s(x_2)\right)}{u_s(x_2)} \quad \text{for all } y \text{ in the outer region.} \tag{42}$$

The velocity $u(x,y)$ is written in this way to specify that the scaled velocity comparisons are made at the equivalent scaled $y/\delta_s(x)$ values and not at the equivalent y-values. The Eq. 42 definition is slightly modified from Schlichting's[2] usual definition of similarity by changing "for all y" to "for all y in the outer region" (the exact definition of the outer region extent is not important in the arguments below).

Defect profile similarity is defined in a similar fashion. Using the above notations, defect profile similarity would therefore be given by when

(43)

$$\frac{u_e(x_1)-u\left(x_1,y/\delta_s(x_1)\right)}{u_s(x_1)} = \frac{u_e(x_2)-u\left(x_2,y/\delta_s(x_2)\right)}{u_s(x_2)} \quad \text{for all } y \text{ in the outer region.}$$

By inspection of Eqs. 42 and 43, it is apparent that defect profile similarity and velocity profile similarity must occur simultaneously if

$$\frac{u_e(x_1)}{u_s(x_1)} = \frac{u_e(x_2)}{u_s(x_2)} \quad . \tag{44}$$

Eq. 44 is an important equation. Not only is it a requirement for simultaneous defect and velocity profile similarity, but this **equivalence requirement also shows up as a criterion for defect profile similarity originally developed by Rotta[26] and Towsend.[27]** More recently, Castillo and George,[28] and Kitsios, *et al*.[29] also derived the same criterion. Castillo and George's derivation was specifically developed to consider outer region similarity. It is the same criterion one obtains for velocity profile similarity (Eq. 42, $y \rightarrow H/2$). Although very different approaches, all of these theoretical formulations end up with $u_e(x)$ as a similarity scaling parameter requirement.

In spite of this unassailable theoretical support for $u_e(x)$ as a similarity scaling parameter, **the literature to date has ignored this theoretical result without explanation** and instead looked for other similarity scaling parameters. Using various experimental data sets, a number of groups explored different scaling velocities that "appear" to show better similarity behavior than $u_e(x)$ as a similarity scaling parameter. For example, based on experimental defect profile comparisons, Castillo and George seemingly reject their own theoretical derivations for $u_e(x)$ to advocate for Zagarola and Smits' $u_{ZS}(x)$ scaling instead. Others, including Panton[36] and Buschmann and Gad-el-Hak,[37] attempted to use experimental profile comparisons to show that $u_{ZS}(x)$ is superior to $u_e(x)$ as a similarity scaling parameter.

Hence, theory says one thing and experimental evidence seemingly says something else. Which is correct? **In this case, it is the theory that is correct.** To understand why this is the case, one must understand how experimental similarity is usually evaluated. What is normally done is to simply plot all of the scaled profiles onto one graph. If the scaled profiles all overlap using the **"**chi-by-eye" test, then the profiles are assumed to be similar. Consider, for example, Figure 20a where some of Österlund's[38] scaled wind tunnel experimental data is plotted at various wall positions. Both Panton and Buschmann and Gad-el-Hak also used some of the Österlund's data to assert that $u_{ZS}(x)$ is the better similarity parameter. Examining Figure 20a by eye, one would have to agree that ***$u_{ZS}(x)$* is very effective at producing similar-like behavior for the defect profile case**. All five profiles plot on top of one another. However, now consider Figure 20b in which the same **exact data and scaling parameters** are used but the data is plotted as velocity profiles. By any measure, the five velocity profiles in Figure 20b do **NOT** display similar behavior.

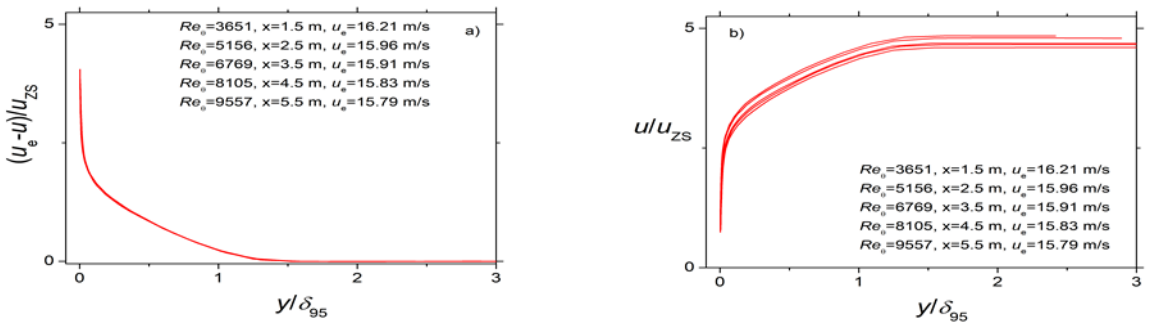

Figure 20: Five Österlund[38] Defect Profiles Plotted using the Zagarola and Smits[33] Scaling Parameters (a) and (b) Five Österlund[38] Velocity Profiles Plotted using the Zagarola and Smits[33] Scaling Parameters

So, what is going on in Figure 20a and b? How can one plot show similarity but not the other? Consider Figure 20b. It is obvious that all five tail regions DO NOT overlap. Let us play the devil's advocate. How can the tail regions in Figure 20b be made to appear to be identical without changing the $u_{ZS}(x)$ scaling parameter? **One way to hide the difference is by subtracting the data's end point from each of the experimental profiles** (Figure 20a). If this is done, then the data sets **tail region will automatically be zero for every profile** thereby ensuring the tail region looks similar for all the defect profiles. Therefore, if you want to inadvertently dupe people into believing that similarity exists, then plot the data as defect profiles. But of course, the tail regions of the scaled velocity profiles, Figure 20b are not similar. By definition, similarity requires the tail regions scaled velocities must be equal which Figure 20b indicates they are clearly not. Similarity must occur in both defect profiles and velocity profiles simultaneously. **You cannot subtract off the endpoint and change the physics of the flow.** This data set does NOT display velocity profile similarity when scaled with $u_{ZS}(x)$ in spite of the fact that Figure 20a appears to display defect profile similarity. Therefore, this data set is not similar when scaled with the Zagarola and Smits scaling parameters.

There is one additional factor[35] particular to the $u_{ZS}(x)$ scaling parameter that tends to ensure the defect profiles at every scaled y-location look similar and not just in the tail region. Plots of $y/\delta_{99}(x)$ versus $u(x,y)/u_{ZS}(x)$ where $u_{ZS}(x) = u_e(x)\delta_1(x)/\delta_{99}(x)$ means all of the curves are normalized by the displacement thickness which is the area under the defect profile. Hence, the area under the plots like Figure 20a all have areas equal to one. For profiles that are taken from locations downstream of each other, plotting scaled profile data with equal areas tends to make the profiles appear to overlap whether they are similar or not. Therefore, the combination of eliminating the tail region disparity combined with the equal area factor means that most data sets will "appear" to be similar when the Zagarola and Smits scaling is used.

When Clauser[32] discovered that defect profiles showed similarity but the velocity profiles did not, the theoretical work of Rotta,[26] Townsend,[27] Castillo and George,[28] and Kitsios, *et al.*[29] was not yet in place. **Their theoretical results indicate that if similarity is present, then $u_e(x)$ must be a similarity scaling parameter for defect profile similarity** (Eq. 44). This means that defect profile similarity and velocity profile similarity must occur simultaneously (Eqs. 42 and 43). In every data set that Weyburne[34,35] examined that other groups have claimed to show defect profile similarity, velocity profile similarity was absent. Attempting to convince

the flow community that there is a problem has proven to be difficult. The visual indication of plots like Figure 20a have convinced even the group that developed a defect profile similarity theory (Castillo and George[28]) that $u_{ZS}(x)$ is a superior scaling parameter. This group and others failed to understand the implication of the theoretical derivations. The bottom line is that much of the research on turbulent boundary layer similarity for the last 70 years is seriously flawed and requires a thorough review. Perhaps the most important conclusion of the search for TBL similarity is that contrary to Castillo and George, Turbulent Boundary Layer similarity is NOT widespread but rare. Unfortunately, this means that developing a generalized approximate TBL velocity profile based on similarity scaling is unlikely to work.

The TBL similarity problem is extensive. The Zagarola and Smits papers,[33] for example, have been referenced over 800 times. The visual proof offered by defect profile plots is so strong that the flow community has **never attempted to explain how the theories of Rotta,[26] Townsend,[27] Castillo and George,[28] and Kitsios, *et al*.[29] are flawed** in requiring $u_e(x)$ be a similarity scaling parameter instead of $u_{ZS}(x)$. Common sense indicates that the flow physics of profile similarity should not be changed by simply replotting the DC shifted data. Yet, the flow community's acceptance to Clauser's defect profile preference over velocity profile similarity has been universal. (To Clauser's[32] credit, the defect profile theories of Rotta,[26] Townsend,[27] Castillo and George,[28] and Kitsios, *et al*.[29] were not yet in place when he did his experimental work).

6.1 Alternative Outer Region TBL Similarity Scaling Parameters

In the same set of papers[34,35] showing how the Zagarola and Smits scaling parameters do not work, Weyburne also showed how the whole profile similarity parameters $\delta_1(x)$ and $u_e(x)$ appear to give reasonable results for a certain limited set of TBL data sets. Four examples were demonstrated. One example is the five Österlund[38] TBL profiles used in Figure 20. In Figure 21, the data is replotted using the $\delta_1(x)$ and $u_e(x)$ scaling parameters. The overlap is not perfect but certainly better than the Zagarola and Smits scaling parameter set result shown in Figure 20b. In a second set of papers, Weyburne39,40 did a simple comparison test using the δ1(x) and ue(x) scaling parameters along with the Prandtl Plus scaling's and the Zagarola and Smits scaling's plots to search for similarity in the outer region of experimental TBL velocity profile data sets. The later paper40 also offers a numerical method for determining whether similarity is present in a set of velocity profiles as opposed to the present "chi-by-eye" examination of graphed data sets. The results indicate that strict whole profile similarity is not evident in any of the datasets that were searched. However, ten datasets were found that displayed "similar-like" behavior when scaled with δ1(x) and ue(x) scaling parameters.39,40

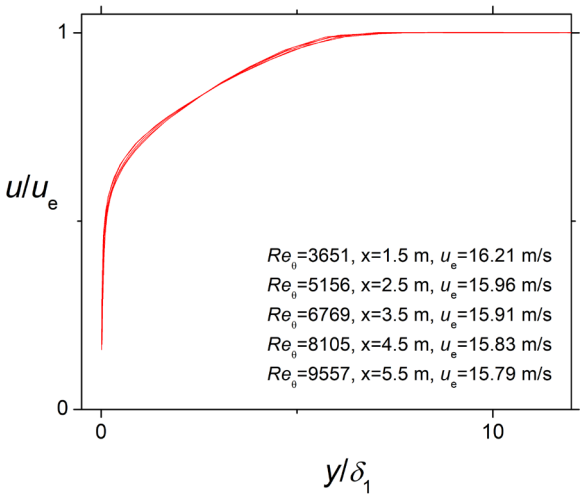

Figure 21: The same Österlund38 TBL Data from Figure 20 but plotted with the Whole Profile Similarity Parameters found by Weyburne21

6.2 The Thermal Profile TBL Similarity Scaling Fiasco

It turns out that the same type of similarity fiasco that has been playing out for the velocity profile has also been repeated for the thermal TBL profile case.[42] Wang and Castillo[43] have developed empirical parameters based on the thermal displacement thickness for scaling the temperature profile of the turbulent boundary layer flowing over a heated wall. They presented experimental data plots that showed similarity type behavior when scaled with their new scaling parameters. However, what was actually plotted, and what actually showed similarity type behavior, was not the temperature profile but the defect profile formed by subtracting the temperature in the boundary layer from the temperature in the free stream. Recently, Weyburne[42] showed that if the same data and same scaling is replotted as just the scaled temperature profile, similarity is no longer prevalent. This failure to show both defect profile similarity and temperature profile similarity is indicative of the same type of failed similarity discussed above for the velocity profile similarity case. The arguments leading to this conclusion are identical in nature to those discussed above. Rather than repeating the arguments, refer to the Wang and Castillo Rebuttal[42] paper instead. The bottom line is that the thermal similarity claims of Wang and Castillo[43] are flawed and should be retracted.

7 THE LOGARITHMIC LAW OF THE WALL EXPLAINED BY A NEW TBL CONCEPTUAL MODEL

In this Chapter, a new conceptual model for the turbulent boundary layer is reviewed. The new model offers a realistic insight into the origin of the Log Law region. The advantage of this new model is that it directly connects experimental observations to the appearance of the Log Law region making it easy to conceptualize.

The "Logarithmic Law of the Wall" pertains to the behavior of the time averaged velocity profile for turbulent boundary layer flow along a wall. The Law of the Wall states that the average velocity for turbulent flow at a certain point above the wall is proportional to the logarithm of the distance from that point to the wall. The name "Law of the Wall" comes from the fact that much of the flow community (see, for example, George[41] and Marusic, *et. al*.[44]) believes this logarithmic behavior is universal for all turbulent flows along interior and exterior walls. The original Log Law derivation was derived independently by Ludwig Prandtl[45] and Theodore von Kármán[46] among others. A good review of the historical as well as fairly recent developments is provided by Buschmann and Gad-el-Hak.[37] In what follows, the first step is to review the traditional conceptual model for the turbulent boundary layer.

7.1 The Traditional Turbulent Boundary Layer Model

The traditional physical model of the structure of the smooth-wall turbulent boundary layer is usually discussed in terms of the properties of the mean velocity profile. The turbulent boundary layer mean profile is normally divided into four sublayers: 1) a viscous linear sublayer closest to the wall, 2) a buffer layer, 3) a logarithmic layer, and finally, 4) the wake outer layer. The Logarithmic Law of the Wall refers to the logarithmic layer. It is supposed that each of these regions' boundaries occurs at a fixed distance from the wall which is measured in terms of the Prandtl Plus thickness values. For example, the location of the boundary between the linear and buffer sublayers is thought to occur at about $y^+ = 5$ Prandtl Plus length units.

This sublayer structure is a finer division than the viscous inner and inertial outer regions often used when discussing the scaling behavior of the turbulent boundary layer. Although there has been no discussion in the literature, presumably, the inner region consists of the first three sublayers and the wake region is the inertial outer region.

The traditional physical model of the TBL has a number of problems. For example, it is known that the low Reynolds number turbulent flows do not have a Logarithmic Law region. Then there is the on-going debate as to what is the proper start and end extent of the Logarithmic Law region (see Marusic, *et. al*.[44] and Örlü[47]). The large scatter in the assignment of the start and stop locations from the literature brings into question the universal picture. Perhaps the most pressing problem is that the physics of the boundary layer is being obscured by this four-sublayer model. For example, reading the literature, one is led to believe that the velocity profile in the so-called linear sublayer behaves linearly. However, if the profiles really behaved linearly in this region, the viscous momentum forces would be zero (the second derivative of the velocity would be zero). In fact, the opposite is true, the viscous momentum forces actually peak in this sub-region. The physics of the Log Law sublayer is similarly opaque. There is no simple physical explanation for the appearance of this sublayer in the traditional model.

7.2 The New Turbulent Boundary Layer Conceptual Model

Rather than the fixed location sublayer model presently employed, Weyburne[48,49] proposed a new model of the turbulent boundary layer that returns to the two-layer viscous inner region and the inertial outer region. The thickness and location of the regions are not fixed but are defined by the moment-based[7,8] thickness and shape parameters. These moment-based thickness parameters are experimentally accessible. The new model also incorporates the experimentally accessible instantaneous wall shear stress. In principle, the instantaneous wall shear stress can be experimentally measured at any location along the wall. Experimental observations indicate that the wall shear stress for TBLs undergo rapid changes (many times a second time scale) due to the chaotic turbulence in the outer region of the boundary layer (see, for example, Obi, *et. al.*[50]). This outer region turbulence penetrates far enough into the inner region to cause this rapid variation in the wall shear stress.

The first key insight provided by the new TBL model is that this rapid time-varying change in the wall shear stress induces rapid, **quantifiable** changes in the thickness and shape of the viscous region in the turbulent boundary layer. The relationship between the wall shear stress and the viscous layer of the wall-bounded turbulent boundary layer is detailed in a paper by Weyburne[8] and summarized in the Boundary Layer Thickness Chapter. To understand how the instantaneous viscous region thickness and shape is related to the instantaneous wall shear stress, one has to look at the momentum balance equations. The x-momentum balance equation tells us the viscous forces will be significant where the second derivative of the velocity $u(x,y)$ is significant. For laminar flow, for example, the second derivative of the Blasius[6] velocity is plotted in Figure 22.

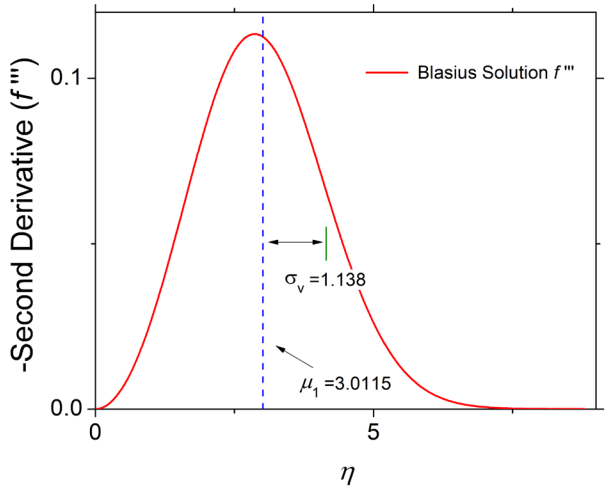

Figure 22: The Second Derivative of the Blasius Velocity Profile showing the Mean Location μ1 and the Boundary Layer Width σv

The instantaneous turbulent boundary layer profiles are not experimentally available but presumably look similar. The Gaussian-like shape in Figure 22 is what led to the adoption of the standard probability moment method for describing the boundary layer thickness and shape.[22] The second derivative integral moments provide a way to describe the thickness and shape of the region where viscosity is important. Included on this plot is the location of the viscous mean location, μ_1, and the viscous boundary layer width, σ_v. The important part to

understand is that it is easily verified that the second derivative instantaneous mean location and instantaneous width are both directly (inversely) proportional to the instantaneous wall shear stress value. Following standard probability practice, the mean, or in this case the mean location $\mu_1(x,t)$, at time t can be shown to reduce to
(

$$\mu_1(x,t) = \frac{\upsilon u_e(x,t)}{\tau_w(x,t)} \quad , \tag{45}$$

where υ is the viscosity, τ_w is the wall shear stress, and $u_e(x)$ is the velocity at the boundary layer edge. The boundary layer width σ_v can **also** be shown to be proportional to the instantaneous wall shear stress along with the instantaneous displacement thickness.[8] What this means is that if the instantaneous wall shear stress and displacement thickness is measured at some point on the wall, then the location and width of the viscous force for the TBL at that precise time and location can be calculated. Actual TBL experiments indicate that the wall shear stress at any point on the wall is undergoing wide excursions over time (see, for example, Obi, *et. al.*[50]). This, in turn, **means that the second derivative profile width is undergoing compression and expansion as the mean location moves toward the wall or away from the wall in lock step with the wall shear stress changes.** This is a key link between experimental observations and what is physically happening in the near wall region of the boundary layer.

Imagine now that the instantaneous second derivative profile is time averaged. It is the time averaged profile that is usually discussed in the literature. **The second key insight of the new model was the observation that the time-averaged tail of the viscous region is decaying very slowly and extends all the way to the Log Law region.** Conventional thinking is that the viscous sublayer only extends from the wall to about $y^+ \cong 30$ into the fluid whereas the Log Law layer starts much further from the wall. However, plots of the velocity profile side-by-side with plots of the second derivative of the velocity, make it clear that the Log Law region is not a separate sublayer but is in fact an integral part of the tail region of the viscous second derivative profile. To show this, high quality experimental turbulent boundary layer velocity profile data sets that showed Log-Law-type behavior can be numerically differentiated twice and compared to the second derivative of the Log Law velocity profile (see Weyburne[48,49]). An example is shown in Figure 23a for data from Österlund.[38] In Figure 23b the associated velocity profiles are shown. Note that the logarithmic overlap regions are the same in both cases. The key point is that the logarithmic region of the TBL is not some overlap region or a sublayer as traditionally advocated, but it is instead the tail part of the viscous region obtained by time-averaging the instantaneous velocity profile. Hence, the new model puts us back to the two regions, inner (viscous) and outer (inertial) region model. It now becomes clear why the first three layers of the traditional TBL model all have the same scaling parameters (Prandtl Plus) and that is because the three closest sublayers are not separate layers but instead are all part of the inner viscous region.

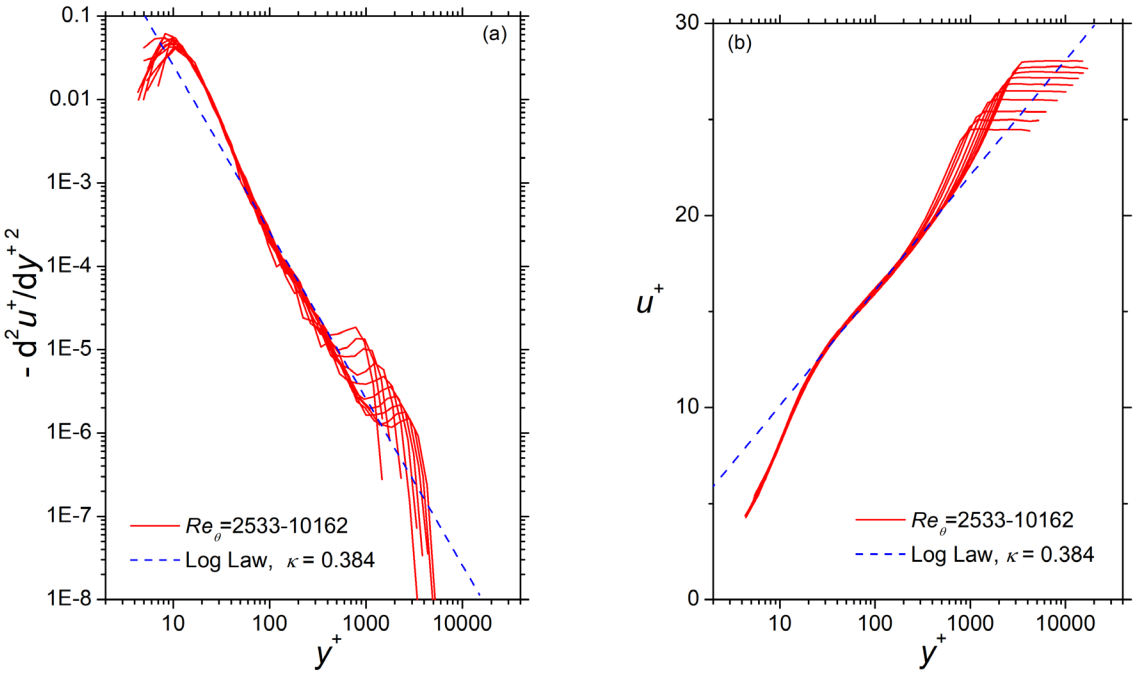

Figure 23: The Österlund[38] SW981129 Second Derivative Profiles plotted in Plus Units (a) and (b) The Österlund[38] SW981129 Velocity Profiles plotted in Plus Units

Examination of Figure 23a reveals that the **Log Law region is 2 or 3 orders of magnitude lower than the viscous peak**. This is why conventional thinking holds that the viscous sublayer only extends from the wall to about $y^+ \cong 30$. So, how can this many orders of magnitude variation still be considered the viscous region? The reason is related to the time-averaging process. There is a whole spectrum of instantaneous μ_1 and σ_v values, including values that put the instantaneous second derivative curve deep into the Log Law region. However, **the probability of having these low wall shear stress values over time is low**. The net result is that the time-averaged viscous region falls off as $1/y$ in the Log Law region since there are fewer instantaneous velocity profiles whose wall shear stress values push the second derivative curve into this region. Hence, when the time-average is done, this region appears to be much diminished when in fact it is due to the time-averaging process.

7.3 The Origin of the Log Law Layer

What is exciting about the new model is that it opens up a whole new way to experimentally attack the origin of the Log Law layer of wall-bounded turbulent boundary layers. The major unknown in the new model is the shape of the instantaneous velocity profile, and in turn, the shape of the instantaneous second derivative profile. Together with the wall shear stress measurement, it might be possible to develop an instantaneous velocity profile theoretical model that takes into consideration the time-varying wall shear stress. The time-based probability distribution function of the wall shear stress values is experimentally accessible, which combined with an instantaneous velocity profile model, should make it possible to construct the time averaged velocity profile for the TBL. It might be possible to show the time averaging process results in logarithmic behavior in the tail region of the viscous inner region.

Along these lines, in the earlier effort Weyburne[48] tried to construct a time-averaged second derivative profile using laminar-like instantaneous profiles with a range of wall shear stress values. He speculated that the tail of the turbulent instantaneous second derivative profile might have the same Gaussian like-tail as what occurs for laminar flow. From a physical perspective, there is a good reason to assume that the second derivative profile of turbulent flow should decay in the same Gaussian-like decay behavior of laminar flow into the fluid. The timescales for the turbulent motion are many orders of magnitude longer than the time scales normally associated with the molecular diffusion time scales of the viscous forces. Hence the main factor affecting the shape of the viscous region of the velocity profile (besides fluid properties) will be the instantaneous wall shear stress value and the free stream velocity. In the end, Weyburne found that the Gaussian-like decay behavior did **not** produce the slow decay behavior seen in the average TBL velocity profile. What is needed to continue along this path is direct numerical simulations studies of the TBL. It should be possible to determine the instantaneous velocity profile and then bin the profiles by wall shear stress value to obtain an averaged bin profile. By convolving with bin averaged profile with the wall shear stress PDF, it might be possible to construct the time averaged profile and from this show that the Log Law region results from the binning averaging process.

7.4 The New TBL Concept and Experimental Measurements

In the traditional inner region boundary layer model, the sublayers are supposed to have fixed boundaries at specific distances from the wall in terms of the Prandtl Plus thickness values. The model supposes that these assignments are universal for all wall-bounded turbulent boundary layers. However, this idea of fixed boundaries at fixed locations is pure conjecture, and an untestable conjecture due to the fact that it **is not** possible to actually measure the location and extent of these sublayers. The controversy over proper start and end extent of Logarithmic Law region (see Marusic, *et al*.[44] and Örlü[47]) illustrates the fact that there has never been a way to precisely define or physically measure the boundary **sub-layer extents**. The bottom line is that **the whole sub-region model has no basis in theory, it is all based on suppositional observations of scaled experimental velocity profile curves.**

If we are to move away from a universal fixed boundary picture of the turbulent boundary layer then what is needed is a way to actually physically describe and measure these regions based on experimentally accessible information. **The new turbulent boundary layer description** discussed in the Boundary Layer Thickness and Shape Chapter **accomplishes this goal**. The time-averaged second derivative based viscous mean location, μ_1, and the time-averaged viscous boundary layer width, σ_v, are both experimentally accessible from velocity profile measurements and/or wall shear stress measurements. Thus, in the new TBL conceptual model, the location and shape of the time averaged viscous sublayer are measured directly. If the accumulated experimental evidence indicates that the location is fixed and universal, then so be it.

There are a number of advantages of the new inner region length scaling parameters as compared to the Prandtl Plus parameter that are discussed in more detail in the next section.

8 A PRANDTL PLUS SCALING PARAMETER ALTERNATIVE

In this Chapter, we re-examine the inner region scaling for turbulent boundary layers developed by Prandtl.[45] There has been universal consensus that the "Prandtl Plus" scaling applies to the inner region of both interior and exterior turbulent boundary layer flows. However, recent research by Weyburne[51,52] uncovered a serious theoretical flaw that necessitates a re-examination of the Prandtl Plus scaling. This research is first reviewed and then the case for a scaling parameter set based on the moment method to replace[53] the Prandtl Plus scaling parameters is outlined. Although it is claimed as a replacement, it is actually a case where the new parameters incorporate the essence of the Prandtl Plus parameters into the integral moment method (Chapter 5) for describing the thickness and shape of the velocity profile. The main advantage of doing this is that it eliminates the theoretical problem encountered with the Prandtl Plus parameters while behaving identically on experimental data.

8.1 Are the Prandtl Plus Scaling's Universal?

The idea of velocity profile similarity is well known for laminar flow along a wall. For turbulent flow along a wall, it is generally acknowledged (Marusic, *et. al*.[31]) that whole profile similarity does not exist (exception: sink flow). That is, "... not even the mean velocity can be described from the wall to the free stream by a function of a single similarity variable." So, instead of looking for similarity over the whole profile, researchers started looking for similarity in just the inner or outer regions. The scaling in the outer region of the turbulent boundary layer region was discussed in the TBL Chapter. For the inner region, there has been no disagreement, until recently, about the proper similarity scaling for the region of the turbulent boundary layer near the wall where viscosity is important. There has been universal consensus that the parameters proposed by Prandtl,[45] the so-called Prandtl Plus parameters, are the proper scales.

The belief that the Prandtl Plus scaling is the proper scaling for all exterior and interior turbulent boundary layers is tied to the Logarithmic Law of the Wall. It is actually the Logarithmic Law of the Wall that is considered universal (see discussion in George[43] and Marusic, et. al.[44]) and it so happens that the Logarithmic Law of the Wall subsumes the Prandtl Plus scaling. Given that this is considered a law of nature, **one would expect that the Logarithmic Law of the Wall would have been extensively verified both theoretically and experimentally. However, this is not the case.** Consider the experimental verification. Marusic, *et. al.*[31] has indicated that the Logarithmic Law of the Wall verification is not possible at the present time due to the limitations of the experimental accuracy of the wall shear stress. The wall shear stress has proven to be very difficult to measure experimentally. For that reason, most experimental determinations of the wall shear stress come in the form of the friction velocity determined by the Clauser[32] Chart method. The Clauser Chart method assumes the Logarithmic Law of the Wall holds so plots of inner region of turbulent boundary layer velocity profiles using this method will always show similar-like behavior. This had led many in the flow community to falsely believe the Logarithmic Law of the Wall actually has been verified. This is reinforced by a study by Marusic, *et. al*.[44] that offered a number of recent experimental results on boundary layers, pipe flow, and the atmospheric surface layer that support the existence of a universal logarithmic region. While the data sets in the study may offer support for universality, it is obviously not proof since independent measurements of the wall shear stress were not performed in all cases.

Hence, in spite of the connotation as a law of nature, the Logarithmic Law of the Wall and the Prandtl Plus scaling's have NOT been verified experimentally.

Without experimental verification, then one would expect that the Logarithmic Law of the Wall and the Prandtl Plus scaling's would have been verified theoretically. Although there have been many theoretical derivations of the Logarithmic Law of the Wall, the derivations are not the same as theoretical proof that that the Prandtl Plus parameters must be similarity parameters for all wall-bounded turbulent boundary layer flow. In fact, there is no theoretical proof that the Prandtl Plus scaling's must be similarity scaling parameters for the inner region of the TBL (the proof offered by Jones, *et. al.*[54] is flawed, see Appendix Weyburne[23]). To the contrary, George[43] recently made a constant shear stress theoretical argument against the universality the Logarithmic Law of the Wall for boundary layer flows along a wall versus pipe/channel flows. This was followed by a different potent theoretical argument offered by Weyburne[51,52] against the universality of the Logarithmic Law of the Wall AND the Prandtl Plus scaling's. Using an α and β based Falkner-Skan momentum equation approach applied to the inner region of turbulent boundary layer, Weyburne[51] showed that Prandtl Plus scaling's ONLY show similar behavior for the turbulent sink flow case and do NOT work for the general Falkner-Skan flow case.

Weyburne's argument is based on the turbulent boundary layer version of the Falkner-Skan[17] momentum equation. In his Falkner-Skan similarity approach, a stream function is constructed by taking the product of the x-dependent length and velocity scaling parameters times a scaled y-dependent functional (see Panton,[20] p. 543). For the turbulent boundary layer version, the velocities are cast into the average velocities and the deviation from the average value using the Reynolds decomposition approach. The resulting mass and momentum conservation equations for the average velocities reduce to an equation that looks like the laminar flow expressions but having additional terms involving the deviation from the average stress terms. The stream function approach is an equivalent but more elegant way of nondimensionalizing the momentum equations compared to the defect velocity profile approach of Rotta,[26] Townsend,[27] and Castillo and George[28] since it automatically incorporates the mass conservation equation. For similarity to be present at various stations along the wall, all of the x-dependent terms of the nondimensionalized momentum equations must change proportionally as one moves along the wall or, equivalently, the ratios of the x-dependent terms must be constant. The Falkner-Skan flow α and β terms are examples of the constant ratio terms. The turbulent boundary layer version of the Falkner-Skan β term is

$$\beta = \frac{\delta_s^2}{\nu}\frac{du_s}{dx} \quad , \tag{46}$$

where ν is the kinematic viscosity, $\delta_s(x)$ is the similarity length scaling parameter, and $u_s(x)$ is the similarity velocity scaling parameter. This term is identical to the Falkner-Skan laminar flow β term. With the α and β terms in hand, Weyburne[51] made the observation that if the Prandtl Plus scaling was truly universal, then Prandtl Plus scaling parameters should work for the inner region of the Falkner-Skan turbulent flow case. That is, if assume Prandtl Plus scaling parameters are correct scaling parameters for the inner region, then

$$\delta_s(x) \;=\; \frac{\nu}{u_\tau(x)} \quad \text{and} \quad u_s(x) \;=\; u_\tau(x) \quad , \tag{47}$$

where u_τ is the friction velocity. The turbulent boundary layer β term, Eq. 47 then becomes

$$\beta \;=\; \frac{\nu}{u_\tau^2}\frac{du_\tau}{dx} \quad . \tag{48}$$

The solution to this differential equation for a constant β is that $\boldsymbol{u_\tau}$ **must behave as 1/**$\boldsymbol{x}$ where x is distance along the wall in the flow direction. This behavior, together with the calculated $\alpha = 0$ result (not shown, see Weyburne[51]), are characteristic of sink flow, flow in a converging/diverging channel. **The Prandtl Plus scaling's, therefore, are NOT solutions for general turbulent Falkner-Skan flows along a wall.**

The result is incontrovertible: either the stream function approach to similarity is flawed OR the Prandtl Plus scaling's are **NOT** similarity scaling parameters for **general** Falkner-Skan flows along a wall. Although there has been no existence proof offered for the stream function approach to similarity or the equivalent defect profile approach, there has been no literature indicating that these approaches are flawed or have problems.

8.2 Is There a Better Alternative to the Prandtl Plus Scaling's?

8.2.1 The Falkner-Skan Alternative to the Prandtl Plus Scaling's

In the same paper[51] that the Falkner-Skan problem with the Prandtl Plus scaling was discussed, a new inner region similarity scaling parameter set was introduced by essentially reverse engineering the Prandtl Plus parameter failure. Both the new parameter set and the Prandtl "Plus" scaling parameters are based on the one wall parameter that is experimentally accessible; the wall shear stress. The wall shear stress is directly proportional to the derivative of the velocity, $du(x,y)/dy$, evaluated at the wall. Prandtl[45] converted this velocity derivative into a length scale and a velocity scale by combining it with the kinematic viscosity. The Prandtl method of creating a length scale from the wall shear stress is not the only way to do it. The development of the new reverse engineered parameters begins with realization that while the **Prandtl Plus parameters have a big theoretical problem, experimentally, the wall shear stress determined by the Clauser chart method has been shown to be is reasonably consistent** (but unverified) **with other direct experimental measurements**. This appears to be true even for general turbulent boundary layer Falkner-Skan type flows. So, how do we resolve the theoretical failure but the experimental success?

Weyburne[51] approached this problem by first reverse engineering the theoretical failure. The idea is to define a new velocity scaling parameter $u_0(x)$, and a new length scaling parameter $\delta_0(x)$, based on an expression found by Weyburne.[53] The first step starts with the ratio of the scaling parameters. It can be proven that **for similarity to occur in a set of velocity profiles** for 2-D boundary layer flow, **the ratio of the similarity velocity scaling parameter to the similarity length scaling parameter must be proportional to the friction velocity squared divided by the kinematic viscosity** (see Weyburne,[23] Eq.10). That is, the ratio is given by

$$\frac{u_0}{\delta_0} \propto \left.\frac{du}{dy}\right|_{y=0} = \frac{u_\tau^2}{\nu} = \frac{\tau_w}{\rho\nu} \Rightarrow \delta_0 = \frac{c\nu u_0}{u_\tau^2} \quad , \tag{49}$$

where c is a proportionality constant. There are two facts to notice here. First, the Prandtl Plus scaling's also satisfy this condition. Secondly, this definition by itself does not fully define the new parameters. To do that, Weyburne revisited the Prandtl Plus failure. The failure came in the form of not satisfying the Falkner-Skan α and β terms. So, in addition to Eq. 49, $u_0(x)$ and $\delta_0(x)$, are required to make the Falkner-Skan α and β terms be constants. Substituting Eq.49 into Eq. 46, we require that $u_0(x)$ be given by

$$c^2 u_0^2 \frac{du_0}{dx} = \frac{\beta u_\tau^4}{\nu} \quad , \tag{50}$$

where β, ν, and c are constants. The new scaling parameters given by Eqs. 9.4 and 9.5 therefore satisfy the part of the flow governing equations approach to similarity which the Prandtl Plus scaling's do not, *i.e.* they should work for general Falkner-Skan flows. For flows obeying Falkner-Skan power law length and velocity scales, it is easily demonstrated that the x-behavior for $u_\tau(x)$ recovered from Eq. 50 is the same as the original Falkner-Skan laminar flow result.

8.2.2 The Integral Moment Parameters as Alternatives to the Prandtl Plus Scaling's

Eqs. 49 and 50 address the expected x-behavior of the new velocity scaling parameter, $u_0(x)$, and the new length scaling parameter, $\delta_0(x)$, in terms of the x-behavior of the wall shear stress. They do not address the identity of these parameters. In a follow-on paper, Weyburne[53] went about identifying these new inner region scaling parameters. It turns out the new length scaling parameter is one of the integral moment method parameters that defines the thickness and shape of any 2-D wall bounded boundary layer region. Using the second derivative based moment method, Weyburne[53] showed that the identity of the length scaling parameter is the second derivative mean location $\mu_1(x)$ and the velocity at the boundary layer edge $u_e(x)$ is the velocity scaling parameter for the inner region of the turbulent boundary layer, including the Log Law region.

The second derivative mean location parameter $\mu_1(x)$ is formally defined as the first y-moment about zero of the second derivative central moments (see Chapter 5, Eqs. 17 and 18). It is easily verified[7,8] that $\mu_1(x)$ is given by

$$\mu_1(x) = \frac{\nu u_e(x)}{u_\tau^2(x)} = \frac{u_e(x)}{\left.\frac{du(x,y)}{dy}\right|_{y=0}} = \frac{\upsilon u_e(x)}{\tau_w} \quad . \tag{51}$$

where υ is the viscosity. This means that the new length scaling parameter is inversely proportional to the wall shear stress. Comparing Eq. 49 to Eq. 51, it is evident that the identity of $u_0(x)$ and $\delta_0(x)$ are $\mu_1(x)$ and $u_e(x)$.

Comparing the Prandtl parameter set and the New set, it is evident that the new parameter set $\mu_1(x)$ and $u_e(x)$ satisfies the Falkner-Skan similarity condition for general Falkner-Skan flows whereas the Prandtl Plus parameter set does not. Consider the Prandtl Plus Falkner-Skan problem with the Falkner-Skan Eq. 48 β term. For the New parameter set, the equivalent Falkner-Skan β term is

$$\beta = \frac{\mu_1^2}{\nu}\frac{du_e}{dx} = \nu\frac{u_e^2}{u_\tau^4}\frac{du_e}{dx} \quad . \tag{52}$$

Assuming the resulting β is a constant, then Eq. 52 represents a similarity requirement for the x-behavior of $u_e(x)$ and $u_\tau(x)$. However, the primary significance of this equation is that it has no direct restriction on the behavior of $u_\tau(x)$, unlike the Prandtl Plus parameter Eq. 48 which does.

There are other advantages of the New parameter set compared to the Prandtl Plus set. Consider the length scaling parameters. On the one hand for the Prandtl Plus scaling's, we have ν/u_τ. The best that can be said about this parameter is that it has the right units. On the other hand, for the new set, the length parameter $\mu_1(x)$ is intimately tied to the physics of the viscous region of any 2-D boundary layer flow. It is directly derived as an integral of the momentum balance equation. The viscous region of a boundary layer is defined by the region of the velocity profile where the second derivative of the velocity is important (see Chapter 5). Using the integral moment method[7,8] to define the shape and thickness of this region involves taking integrals evaluated at the wall. The integral of the second derivative evaluated at the wall results[50] in the wall shear stress related **mean location $\mu_1(x)$** (Eq.51). **Thus, the new length scale can be traced directly to the physics of the viscous region.** It is also part of a whole system of related length and shape parameters that describe the velocity profile formed by 2-D fluid flow along a wall.

A related advantage of the New parameter set has to do with the extent of applicability. For the Prandtl Plus parameters, the extent of applicability is tied to the extent of applicability for the Logarithmic Law of the Wall. This was touched on in Chapter 8 but the fluid flow community has had the problem that it is not clear over what region of the velocity profile the Plus parameters are applicale.[44,47] For the New parameter set, the range of applicability is from the wall to some viscous boundary layer thickness (Chapter 5) value determined from $\mu_1(x)$ and $\sigma_v(x)$. With the second derivative moments, it is easily determined over which part of the velocity profile that the viscous forces are important.

The advantages of the New parameter set do not end there. A further advantage of the New parameter set is that it is possible to prove that if similarity is present in a set of velocity profiles, then the length scaling parameter $\mu_1(x)$ is a similarity scaling parameter for any 2-D boundary layer flow.[23] Thus, for turbulent sink flows and laminar flows, if similarity is present in a set of velocity profiles, then $\mu_1(x)$ and $u_e(x)$ must be similarity scaling parameters. On the other hand, the Prandtl Plus scaling's have never been proven to be similarity scaling parameters for any set of velocity profiles (the proof offered by Jones, *et. al.*,[54] is flawed, see the Appendix of Weyburne[23]).

It should be emphasized that strict similarity can only be expected for data sets displaying whole profile similarity. Whole profile similarity of the turbulent boundary layer, with exception of sink flows, has never been observed. Hence, as is the case with the Prandtl Plus parameters, data sets scaled with the new similarity parameters are, at best, only approximately similar (see Weyburne[52]). However, both parameter sets are intended to scale the near wall region where viscosity is important. In fact, the viscosity is important in all near-wall boundary layer situations including **laminar boundary layers**. For laminar flow, the viscous forces are important through the entire boundary layer region. Any near wall scaling parameters should therefore also work for this case. As a test, experimental CFD simulations[5] for exterior-like laminar flow on a thin flat plate are presented in Fig. 9.1a and 9.1b (see Chapter 3). The results are striking. All seven profiles for the new set show complete overlap. It is hard to see but there really are seven curves in Fig. 9.1a. Recall Weyburne[23] theoretically proved that if similarity is present in a set of velocity profiles, then $\mu_1(x)$ and $u_e(x)$ must be similarity scaling parameters that work. Fig. 9.1a is the experimental proof. Advocates for the Prandtl Plus parameter set must explain this huge difference for laminar flow boundary layers. It is now apparent why the Blasius scaling parameters are used for laminar flow and the Prandtl Plus scaling for turbulent flows. The Prandtl parameters just do not work very well for laminar flows. This puts Plus parameter advocates in a very difficult situation. They need to explain why the Prandtl Plus do not work very well but the New parameter set is bang on. As opposed to the Prandtl set, for the New set, it is possible to show that the ratio between the Blasius thickness parameter and $\mu_1(x)$ must be a constant.[8] The bottom line is that the New set works for laminar flow and the Plus parameters do not.

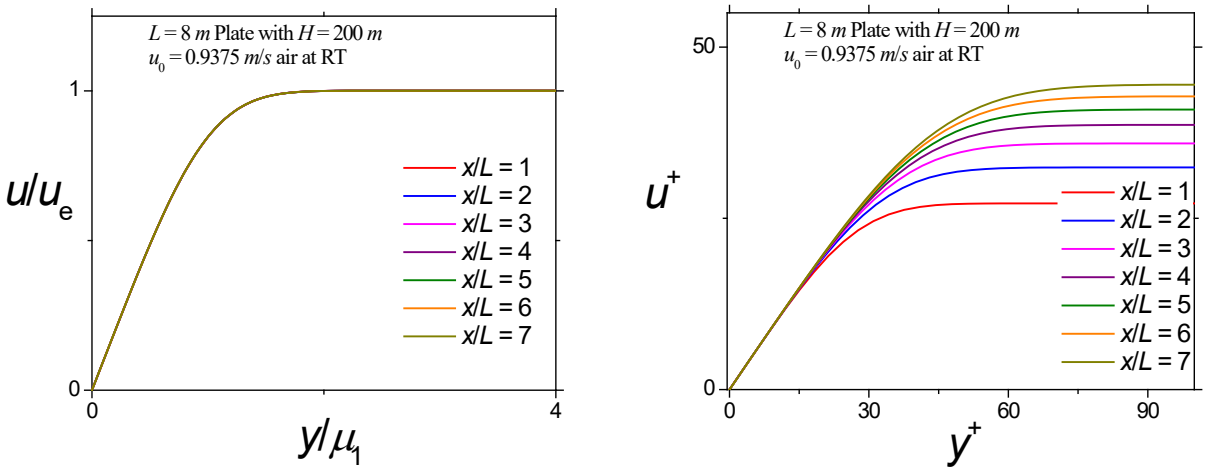

Figure 24: Seven CFD Laminar Flow Profiles scaled using the New Scaling Parameters (a) and (b) Seven CFD Laminar Flow Profiles scaled using the Prandtl Plus Scaling Parameters

The New set is superior for laminar flow boundary layers, but what about the experimental scaling performance for the turbulent boundary layer? What is normally done to discover similar behavior in experimental data is to plot all of the scaled velocity profiles on one graph and use "chi-by-eye" to decide whether similarity is present. Weyburne[51,53] has compared a number of experimental datasets and demonstrated that both sets appear to work similarly. In fact, if the Rotta[26] constraint, $u_\tau(x) / u_e(x)$ = constant, holds then the results will appear identical. The key to

this is realizing that multiplying both the $\mu_1(x)$ and $u_e(x)$ based x and y axes scaling parameters (see Eq. 51) by the factor u_e/u_τ results in the Prandtl Plus scaling variables! Hence, the relative relationships between the plotted curves for the two parameter sets will appear identical as long as the Rotta constraint holds. The actual x-y scales will be different but the plotted curves relative to each other will be identical.

The fact that the experimental results between the two parameter sets are very similar emphasizes that they have one important factor in common; the length to velocity scaling parameter are both directly proportional to the wall shear stress. The Prandtl method of creating a length and velocity scale from the wall shear stress is one way to do it and the New set is another. Stepping back and taking the long view, it appears that the Prandtl Plus theoretical problems can be traced to this attempt to convert one experimental parameter into two scaling parameters. In experimental practice, the Prandtl Plus parameters seem to work just as well for **general Falkner-Skan flows as sink flow** even though theory says they should not. Hence, the Falkner-Skan theoretical problem discussed above with the Prandtl Plus parameters is **not** substantiated by experimental results. This means the one-experimental-to-two-scaling-parameter approach of Prandtl imposes a **theoretical limit to the applicability of the parameters** that does not appear to be substantiated by experimental results. On the other hand, the New parameter scaling set proposed by Weyburne[53] does not suffer from this theoretical short coming.

8.2.3 A New Logarithmic Law of the Wall

When all is said and done, the main importance of trying to cast the Logarithmic Law of the Wall as a law of nature is to provide justification for extracting the wall shear stress from experimental turbulent boundary layers velocity profiles. It is very difficult to measure the wall shear stress experimentally. It is also difficult to measure the velocity profile very close to the wall. The logarithmic region extends further out from the wall due to the slow decay of the averaged second derivative velocity profile which makes it possible to extract the wall shear stress if the Log Law holds true. However, it is worth taking a close look at the various derivations of the Log Law. The derivations only indicate that the interaction of the inner region and outer regions means the velocity profile at the junction between these regions must be logarithmic or maybe a power law. Note that **NONE** of the derivations specifically requires that the scaling parameters must be the Prandtl Plus parameters. As such, the question then becomes is it possible to develop a similar logarithmic function using the New parameter set? A new logarithmic function to approximate the velocity profile would look like

$$\frac{u(x,y)}{u_e(x)} \cong a + b\ln\left(\frac{y}{\mu_1}\right) = a + b\ln\left(\frac{yu_\tau^2(x)}{\nu u_e(x)}\right), \tag{53}$$

where a and b are constants.

So how good is the New Log Law? In Table 1 a and b are some fitting results to DNS experimental data[55] at different Re_θ. The fits were done over the same profile range that advocates of the Log Law reccomend.[44] The results indicate neither Log Law correctly predicted the friction velocity. More importantly, examination of the **residual plots** (not shown) indicate

neither Logarithmic function is correctly predicting the velocity profile. However, it does seem that New Log Law's adjusted R squared values indicate the new fits are significantly better.

Table 1. Results to Fits to Six CFD Turbulent Flow Profiles using the New Log Law (a) (b) Results to Fits to Six CFD Turbulent Flow Profiles using the Old Log Law

New Log Law			Old Log Law		
Re_θ	% error	adj-R^2	Re_θ	% error	adj-R^2
4000	1.1	0.9987	4000	1.7	0.9922
4500	0.5	0.9995	4500	1.5	0.9929
5000	-0.2	0.9994	5000	1.5	0.9927
5500	-1.2	0.9995	5500	1.5	0.9940
6000	-1.7	0.9994	6000	1.4	0.9931
6500	-2.2	0.9994	6500	1.5	0.9938

A few other comparisons to experimental data have been made, and truthfully, this New Log Law is probably not better than the old Log Law. However, the point is that the neither of these so-called Log Laws are directly supported by theory that ties in the scaling parameter identity. No amount of experimental fitting will suffice until a convincing theory is developed. Calling something a law of nature should require a much higher level of verification than has been employed to date. It is better to treat these logarithmic functions as at best good approximations at this point in time.

9 ACKNOWLEDGMENT

The work summarized in this document was completed through the support of the Air Force Research Laboratory and Gernot Pomrenke at the Air Force Office of Scientific Research.

10 REFERENCES

[1]L. Prandtl, "Über Flüssigkeitsbewegung bei sehr kleiner Reibung," Verhandlungen des Dritten Internationalen Mathematiker-Kongresses in Heidelberg 1904.

[2]*H. Schlichting,* Boundary-Layer Theory*, 7*th *ed., McGraw-Hill, New York ,1979.*

[3]D. Weyburne, "A Boundary Layer Model for Unbounded Flow Along a Wall," Air Force Tech Report: AFRL-RY-WP-TR-2020-0004, https://discover.dtic.mil, Accession # AD1091170, 2020.

[4]D. Weyburne, "The Unbounded and Bounded Boundary Layer Models for Flow Along a Wall," Air Force Tech Report: AFRL-RY-WP-TR-2020-0005, https://discover.dtic.mil, Accession # AD1094086, 2020.

[5]D. Weyburne, "A New Conceptual Model for Laminar Boundary Layer Flow," Air Force Tech Report: AFRL-RY-WP-TR-2020-0006, https://discover.dtic.mil, Accession # AD1091170, 2020.

[6]H. Blasius, "Grenzschichten in Flüssigkeiten mit kleiner Reibung," Zeitschrift für Mathematik und Physik, **56**, 1(1908).

[7]D. Weyburne, "New Shape Parameters for the Laminar, Transitional, and Turbulent Velocity Profiles," Air Force Tech Report: AFRL-RY-HS-TR-2010-0016, https://discover.dtic.mil/, Accession # ADA519321, 2010.

[8]D. Weyburne, "New thickness and shape parameters for the boundary layer velocity profile," Experimental Thermal and Fluid Science, **54**, 22(2014).

[9]R. Swanson and S. Langer, "Comparison of NACA 0012 Laminar Flow Solutions: Structured and Unstructured Grid Methods," NASA/TM-2016-219003.

[10]P. Roach and D. Brierlay, "The influence of a Turbulent Free Stream on Zero Pressure Gradient Transitional Boundary Layer Development," in: O. Pirnneau, W. Rodi, I. Ryhming, A. Savill, and T. Truong (Eds.), *Numerical Simulation of Unsteady Flows and Transition to Turbulence*, Cambridge University Press, New York, 1992, pp 319-347. Data from https://www.ercoftac.org/.

[11]M. Drela and M. Giles, "Viscous-Inviscid Analysis of Transonic and Low Reynolds Number Airfoils," AIAA J., **25**, 1347(1989).

[12]J. Jovanović, B. Frohnapfel, E. Škaljić, and M. Jovanović, "Persistence of the Laminar Regime in a Flat Plate Boundary Layer at very High Reynolds Number," Thermal Science, **10**, 63(2006).

[13]U. Ghia, S. Bayyuk, S. Habchi, C. Roy, T. Shih, T. Conlisk, C. Hirsch, and J. Powers, "The AIAA code verification project - Testcases for CFD code validation," AIAA 2010-0125, 2010.

[14]J. Nikuradse, Laminare Reibungsschichten an der längsangetrömten Platte. Monograph, Zentrale f. wiss. Berichtswesen, Berlin, 1942.

[15]J. Lewins, "Beyond the boundary layer: the Blasius paradox," Int. J. Mech. Engr. Educ., **27**, 55(1999).

[16]D. Weyburne, "The Normal to the Wall Pressure Gradient for Blasius and Falkner-Skan Boundary Layer Flow," Air Force Tech Report AFRL-RY-WP-TR-2018-0153, https://discover.dtic.mil/, Accession # AD1063207, 2018.

[17]V. M. Falkner and S. Skan, Aero. Res. Coun. Rep. and Mem. no 1314, 1930.

[18]F. White, *Viscous Fluid Flow*, 2nd edn., McGraw-Hill, 1991.

[19]Y. Cengel and J. Cimbala, *Fluid Mechanics: Fundamentals and Applications*, 2nd edn., TBS, 2009.

[20]R. Panton, *Incompressible Flow*, 4th ed., John Wiley, New Jersey, 2013.

[21]D. Weyburne, "Similarity of the Velocity Profile," AF Tech Report: AFRL-RY-WP-TR-2014-0221, https://discover.dtic.mil/, Accession # ADA609962, 2014.

[22]D. Weyburne, "A mathematical description of the fluid boundary layer," Applied Mathematics and Computation, **175,** 1675(2006). Also D. Weyburne, Erratum, Applied Mathematics and Computation, **197**, 466(2008).

[23]D. Weyburne, "Inner/Outer Ratio Similarity Scaling for 2-D Wall-bounded Turbulent Flows," arXiv:1705.02875 [physics.flu-dyn], 2017.

[24]D. Weyburne, "New thickness and shape parameters for describing the thermal boundary layer," arXiv:1704.01120 [physics.flu-dyn], 2018.

[25]E. Pohlhausen, "Der wärmeaustausch zwischen festen körpern und flüssigkeiten mit kleiner reibung und kleiner wärmeleitung," Zeitschrift für Angewandte Mathematik und Mechanik, **1**, 115(1921).

[26]J. Rotta, "Turbulent Boundary Layers in Incompressible Flow," Prog. Aeronaut. Sci., **2**, 1(1962).

[27]A. Townsend, *The Structure of Turbulent Shear Flow*, 2n edn. (Cambridge University Press, Cambridge, 1956).

[28]L. Castillo and W. George, "Similarity Analysis for Turbulent Boundary Layer with Pressure Gradient: Outer Flow," AIAA J., **39**, 41(2001).

[29]V. Kitsois, A. Sekimoto, C. Atkinson, J. Sillero, G. Borrell, A. Gungor, J. Jiménez and J. Soria, "Direct numerical simulation of a self-similar adverse pressure gradient turbulent boundary layer at the verge of separation," J. Fluid Mech., **829**, 392(2017).

[30]D. Weyburne, "Similarity of the Temperature Profile formed by Fluid Flow along a Wall," arXiv:1603.05062 [physics.flu-dyn], 2018.

[31]I. Marusic, B. McKeon, P. Monkewitz, H. Nagib, A. J. Smits, and K. Sreenivasan, "Wall-bounded turbulent flows at high Reynolds numbers: Recent advances and key issues," Phys. Fluids, **22**, 065103 (2010).

[32]F. Clauser, "The turbulent boundary layer in adverse pressure gradients," J. Aeronaut. Sci. **21,** 91(1954).

[33]M. Zagarola and A. Smits, "Mean-flow scaling of turbulent pipe flow," J. Fluid Mech., **373**, 33(1998). Also M. Zagarola, and A. Smits, "A New Mean Velocity Scaling for Turbulent Boundary Layers," Proceedings of FEDSM'98, Washington D.C., 1998.

[34]D. Weyburne, "The Prevalence of Similarity of the Turbulent Wall-bounded Velocity Profile," arXiv:1412.5129v5 [physics.flu-dyn], 2015.

[35]D. Weyburne, "A Cautionary Note on the Zagarola and Smits Similarity Parameter for the Turbulent Boundary Layer, " arXiv:1507.06951 [physics.flu-dyn], 2017.

[36]R. Panton, "Review of wall turbulence as described by composite expansions," Appl. Mech. Rev., **58**, 1 (2005).

[37]M. Buschmann and M. Gad-el-Hak, "Recent developments in scaling of wall-bounded flows," Prog. Aeronaut. Sci., **42**, 419(2007).

[38]J. Österlund, PhD. Thesis, KTH Royal Institute of Technology, Stockholm, 1999.

[39]D. Weyburne, "Similarity of the Outer Region of the Turbulent Boundary Layer", Air Force Tech Report: AFRL-SN-HS-TR-2010-0013, https://discover.dtic.mil/, Accession # ADA519314, 2010.

[40]D. Weyburne, "Does the Outer Region of the Turbulent Boundary Layer Display Similar Behavior?", arXiv:1706.05236 [physics.flu-dyn], 2017.

[41]D. Weyburne, "A Cautionary Note on the Thermal Boundary Layer Similarity Scaling for the Turbulent Boundary Layer," arXiv:1603.07728 [physics.flu-dyn], 2016.

[42]X. Wang and L. Castillo, "Asymptotic solutions in forced convection turbulent boundary layers," J. of Turbulence, **4**, 1(2003).

[43]W. George, “Is there a universal log law for turbulent wall-bounded flows?”, Philos. Trans. R. Soc. London, Ser. A **365**, 789 (2007).

[44]I. Marusic, J. Monty, M. Hultmark, and A. Smits, “On the logarithmic region in wall turbulence,” J. Fluid Mech., **716**, R3-2(2013).

[45]L. Prandtl, “Über die ausgebildete Turbulenz,” ZAMM **5**, 136(1925).

[46]T. von Kármán, "Mechanische Ähnlichkeit und Turbulenz", Nachr. Ges. Wiss. Goettingen, Math.-Phys. Kl., **5**, 58(1930).

[47]R. Örlü, PhD Thesis, KTH Royal Institute of Technology, Stockholm, 2009.

[48]D. Weyburne, "The Origin of the Log Law Region for Wall-bounded Turbulent Boundary Layer Flows," Air Force Tech report: AFRL-RY-HS-TR-2011-0005, https://discover.dtic.mil/, Accession # AD538378, 2011.

[49]D. Weyburne, "On the Origin of the Log Law Region: Instantaneous Velocity Profile Models." 6th AIAA Theoretical Fluid Mechanics Conference, 10.2514/6.2011-3931, 2011.

[50]S. Obi, K. Inoue, T. Furukawa, and S. Masuda, “Experimental study on the statistics of wall shear stress in turbulent channel flows,” Int. J. Heat and Fluid Flow, **17**, 187(1996).

[51]D. Weyburne, "The Prandtl Plus Scaling Failure and its Remedy," arXiv:1701.02364 [physics.flu-dyn], 2017.

[52]D. Weyburne, "The Prandtl Plus Scaling Approximation for Turbulent Boundary Layer Flows," arXiv:1708.03547 [physics.flu-dyn], 2017.

[53]D. Weyburne, "The Description and Scaling Behavior for the Inner Region of the Boundary Layer for 2-D Wall-bounded Flows," arXiv:1703.02092 [physics.flu-dyn], 2018.

[54]M. Jones, T. Nickels, and I. Marusic, “On the asymptotic similarity of the zero-pressure-gradient turbulent boundary layer,” J. Fluid Mech., **616,** 195(2008).

[55]J. Sillero, J. Jimenez, and R. Moser, Phys. Fluids 25, 105102(2013).

LIST OF ABBREVIATIONS, ACRONYMS, AND SYMBOLS

ACRONYM	DESCRIPTION
2-D	Two-Dimensional
APG	Adverse Pressure Gradient
CFD	Computational Fluid Dynamics
FPG	Favorable Pressure Gradient
RT	Room Temperature
TBL	Turbulent Boundary Layer
ZPG	Zero-Pressure Gradient